Time-dependent earthquake-fire coupling fragility analysis under limited prior knowledge A perspective from type-2 fuzzy probability

Men, Jinkun; Chen, Guohua; Reniers, Genserik

DOI
10.1016/j.psep.2024.01.011

Publication date
2024

Document Version
Final published version

Published in
Process Safety and Environmental Protection

Process Safety and Environmental Protection 183 (2024) 274–292

Contents lists available at ScienceDirect

Process Safety and Environmental Protection

journal homepage: www.journals.elsevier.com/process-safety-and-environmental-protection

Time-dependent earthquake-fire coupling fragility analysis under limited prior knowledge: A perspective from type-2 fuzzy probability

Jinkun Men [a,b,c], Guohua Chen [a,b,*], Genserik Reniers [c,d,e]

[a] Institute of Safety Science & Engineering, South China University of Technology, Guangzhou 510640, China
[b] Guangdong Provincial Science and Technology Collaborative Innovation Center for Work Safety, Guangzhou 510640, China
[c] CEDON, KU Leuven, Campus Brussels, Brussels 1000, Belgium
[d] Faculty of Technology, Policy and Management, Safety and Security Science Group (S3G), TU Delft, 2628 BX Delft, the Netherlands
[e] Faculty of Applied Economics, Antwerp Research Group on Safety and Security (ARGoSS), University Antwerp, Antwerp 2000, Belgium

ARTICLE INFO

Keywords:
Chemical Process Safety
Earthquake-triggered Fire Domino Scenarios
Multi-hazard Coupling Events
Chemical Industrial Parks
Type-2 Fuzzy Possibility Theory
Steel Cylindrical Tank

ABSTRACT

Earthquake-triggered fire domino scenarios (E-FDSs) arise frequently from the interaction between earthquakes and chemical installations, resulting in catastrophic multi-hazard coupling events. The complicated mutually amplified phenomena between natural disasters and chemical accidents significantly aggravates the escalation of domino accidents, which has posed great challenges for modeling and preventing E-FDSs. Under this impetus, this work proposes an advanced type-2 fuzzy probabilistic methodology to obtain the time-dependent failure probability of steel cylindrical tanks (SCTs) subjected to the earthquake-fire sequence. To cope with the limited prior knowledge on E-FDSs, a basic universal is established to describe the fire resistance attenuation caused by the seismic damage. The coupling failure criterion of SCTs is formulated by a type-2 fuzzy time-dependent limit state equation. A credibility-based stochastic simulation algorithm is developed for the hybrid uncertainty analysis (combining ambiguity and stochasticity). The proposed methodology is validated by case studies of a 5000 m^3 fixed roof tank. Compared to the existing accident probability model, the proposed methodology can not only capture the fire resistance attenuation caused by the seismic damage but also provide a dynamic estimation of tank failure probability with respect to the fire exposure time. The proposed methodology can effectively and dynamically capture the accident evolution process, which in turn helps mitigate and prevent the spatiotemporal propagation of domino effects.

1. Introduction

The modern chemical industrial park (CIP) is usually congested with various accident-prone high-risk industrial activities (Bai et al., 2023; Tamascelli et al., 2023; Theofanous, 1981). Due to the flammable, explosive, and toxic characteristics of hazardous chemicals, various cascade, interactional or compound chemical accidents occur frequently, resulting in catastrophic multi-hazard coupling scenarios (Jones et al., 2023; Landucci et al., 2009; Men et al., 2020). As one of the core tasks of process safety and risk management, a lot of efforts have been made to evaluate the probabilistic fragility of hazardous installation units under extreme circumstances (Chen and Reniers, 2020; Men et al., 2023c).

In the early stages of process safety research, scholars have recognized potential hazards coming from technological accidents such as fires and explosions (Cozzani et al., 2005; Cozzani and Reniers, 2013; Cozzani et al., 2009; Schwartz, 1904). The escalation vectors (thermal radiation, blast waves, and fragments) generated by these technological hazards may impose severe damage on adjacent units, of which the propagation of technological hazards between hazardous installation units is well-known as domino effects (Chen et al., 2020; Cozzani et al., 2005; Cozzani and Reniers, 2013). The systemic definition of domino accidents was provided by (Cozzani et al., 2005), i.e. "*an accident in which a primary event propagates to nearby equipment, triggering one or more secondary events resulting in overall sequences more severe than those of the primary event.*" In general, a domino accident can be characterized by three pivotal features: 1) a primary accident; 2) an escalation vector; 3) one or more secondary accidents (Chen et al., 2020; Men et al., 2023b). According to the definition of domino accidents, the core of domino accident analysis is to estimate the domino escalation

* Correspondence to: South China University of Technology, No.381, Wushan Rd.L, Tianhe District, Guangzhou 510640, China.
E-mail address: mmghchen@scut.edu.cn (G. Chen).

https://doi.org/10.1016/j.psep.2024.01.011
Received 15 October 2023; Received in revised form 22 December 2023; Accepted 3 January 2024
Available online 6 January 2024

Table 1
Probit models for domino escalation probability (*ttf*: time to failure (s); *I*: radiation intensity (kW • m^{-2}); V: Vessel volume (m^2); P_s: peak static overpressure on the target equipment (kPa)) (Cozzani et al., 2005).

Escalation Vector	Equipment Type	Probit Model
Fire Radiation	Atmospheric vertical cylindrical vessel	$Y = 12.54 - 1.847\ln_1(ttf) \quad \ln_1(ttf) = -1.128\ln(I) - 2.667 \times 10^{-5}V + 9.877$
	Pressurized horizontal cylindrical vessels	$Y = 12.54 - 1.847\ln_2(ttf)\ln_2(ttf) = -0.947\ln(I) + 8.835V^{0.032}$
Explosion Overpressure	Atmospheric	$Y = -18.96 - 2.44\ln(P_s)$
	Pressurized	$Y = -42.44 + 4.33\ln(P_s)$
	Elongated	$Y = -28.07 + 3.16\ln(P_s)$
	Auxiliary	$Y = -17.79 + 2.18\ln(P_s)$

probability. As shown in Table 1, the *Probit* model is widely used for calculating domino escalation probability (Khakzad et al., 2018; Men et al., 2022b; Xu et al., 2023). A primary accident usually escalates when the escalation vector causes the failure of other equipment units (Chen et al., 2020). Based on historical accident statistics, the *Probit* model provides the probabilistic mapping relationship between the physical damage of equipment units and the intensity of escalation vectors, which is referred to "equipment fragility" (Casson Moreno et al., 2022; Chen et al., 2020).

In addition to the technological hazards accompanying the traditional chemical process, catastrophic cascading events may also arise from the interaction between natural hazards and hazardous installation units, leading to the so-called Na-tech events (*technological hazards triggered by natural hazards*) (Misuri and Cozzani, 2021; Showalter and Myers, 1994). Thus, the damage of equipment units exposed to natural hazards has received increasing attention in recent years as well (Men et al., 2023a; Taghizadeh et al., 2023). Generalized fragility curves were obtained from the historical accident observation data (Cozzani and Salzano, 2004; D'Amico and Buratti, 2018; Huang et al., 2022) or the analytical and numerical approximations (Jia et al., 2017; Mayorga et al., 2019; Yang et al., 2020).

Steel cylindrical tanks (SCTs) are one of the pivotal equipment units in the chemical process industry. SCTs are widely utilized for the storage of various flammable, explosive, and toxic hazardous materials (Djelosevic and Tepic, 2019; Men et al., 2023a; Men et al., 2022b). Thus, studies concerning the fragility analysis of SCTs have been developed extensively (Huang et al., 2023; Men et al., 2023a). Several advanced uncertainty analysis methodologies have been adopted to evaluate the failure probability of SCTs under extreme circumstances. These methodologies include probit regression (Cozzani and Salzano, 2004; Fabbrocino et al., 2005; Zhou et al., 2021), Monte-Carlo simulation (Mayorga et al., 2019; Saha et al., 2016; Wang et al., 2023), and Bayesian analysis (Berahman and Behnamfar, 2009; Caprinozzi et al., 2020; D'Amico and Buratti, 2018). However, these studies can only estimate the damage caused by a single hazard, rather than considering the coupling effects of multiple hazards.

In reality, the evolution of any hazard is not isolated and static (Hillier et al., 2020). In the past decade, a number of scholars have gradually realized the limitations of single hazard studies (Men et al., 2023b; Wang et al., 2020a). This has driven the development of multi-hazard related research. (Chen et al., 2021) proposed a maximum plastic strain criterion-based limit state equation to model tank damage caused by the coupling effects of fire heat radiation and blast fragments. (Ding et al., 2022) developed a Logistic regression-based fragility model for SCTs exposed to fire heat radiation and explosion overpressure. (Li et al., 2022) developed a numerical analytical method to analyze the structural response of SCTs exposed to synergistic blast and fire loads. On this basis, a Probit-based fragility model was proposed to estimate the failure probability of SCTs exposed to simultaneous fire and explosion (Li et al., 2023). (Qin et al., 2020) developed a Bayesian network-based fragility model to capture the dominant failure modes of SCTs in hurricanes-rainfalls-floods coupling scenarios. (Huang et al., 2022) proposed the limit state equation of SCTs exposed to floods and hurricanes, a Monte Carlo simulation-based was proposed to estimate the coupling failure probability.

Existing studies concerning the fragility analysis of SCTs exposed to the sequential loadings of earthquake and fire are limited. The strong ground motion caused by an earthquake may rapidly lead to a series of massive fires in chemical tank farms. More alarmingly, the thermal radiation and the flame impingement generated by fires can also cause damage to adjacent hazardous installation units, of which domino effects are easily triggered. The earthquake-triggered fire domino scenario (E-FDS) is one of the typical multi-hazard coupling events. The mutually amplified phenomena in E-FDSs are significant, as the seismic damage can affect the fire resistance of SCTs. Moreover, the existing uncertainty analysis methodologies require sufficient and reliable prior knowledge to obtain generalized probability mapping relations (Mannering and Bhat, 2014; Men et al., 2023a). Estimating the earthquake-triggered fire domino escalation probability is a complex task, as the relevant prior knowledge is limited by the scale and size of the experiments and simulations. For the existing uncertainty analysis methodologies, the limited prior knowledge is not sufficient to support the further quantitative analysis of earthquake-fire coupling domino accident probability (Fu and Sayed, 2023; Mannering and Bhat, 2014; Men and Zhao, 2023). In addition, static probabilistic model is difficult to capture the time-dependent earthquake-triggered fire domino escalation probability under dynamic extreme circumstances (Huang et al., 2023; Men et al., 2023c).

In this promotion, a hybrid uncertainty analysis methodology that combines both ambiguity and stochasticity is proposed to solve the research gaps mentioned above. A basic *universal* is established to express the knowledge about the coupling failure mechanism of SCTs in E-FDSs, which is the fundamental qualitative description of the fire resistance attenuation caused by seismic damage. According to the basic *universal*, the failure criterion of SCTs exposed to the earthquake-fire sequence is formulated by type-2 fuzzy time-dependent limit state equation, of which uncertainties are modeled by type-2 fuzzy variables. Compared with regular fuzzy variables, the probability distribution functions of type-2 fuzzy variables are also fuzzy, which provides additional degrees of freedom for modeling uncertainties (Men et al., 2022a; Men et al., 2019). Finally, a credibility-based stochastic simulation algorithm is developed for the failure probability estimation in *fuzzy probability space*.

The contribution of this work mainly has four aspects. (1) The time-dependent evolution of earthquake-fire coupling fragility is revealed; (2) An advanced uncertainty analysis methodology is proposed to cope with the limited prior knowledge, achieving a hybrid analysis that combines ambiguity and stochasticity. (3) A type-2 fuzzy time-dependent limit state equation and a credibility-based stochastic simulation algorithm are proposed for dynamic failure probability estimation. Compared to the existing domino escalation probability model, the proposed methodology yields time-dependent coupling failure probability curves, enabling the explainable dynamic failure interval analysis of seismic damaged tanks under fire conditions. (4) A basic type-2 fuzzy universal is established to describe the fire resistance attenuation caused by the seismic damage. Compared to conventional single-hazard fragility analysis methods, the proposed methodology can effectively capture the mutually amplified phenomena between chemical accidents and natural disasters.

The rest of this paper is stated as follows. Some preliminaries about. thermal response analysis and fuzzy possibility theory are stated in Section 2. The multi-hazard coupling dynamic fragility analysis methodology is proposed in Section 3. The methodology demonstration is stated in Section 4. At last, conclusions are drawn in Section 5. This paper includes an additional **Appendix**. The descriptions of related parameters, the theoretical proof, and some illustrations are available in

Fig. 1. Typical earthquake-triggered fire domino scenarios. (a) Massive fires at the TUPRAS Izmit refinery caused by 1999 Kocaeli earthquake (Girgin, 2011); (b) Tanks collapsed due to fires (Scawthorn and Johnson, 2000).

the **Appendix**.

2. Preliminaries

To facilitate model construction, some preliminaries about earthquake-triggered fire domino scenarios, thermal response analysis (Jia et al., 2017; Mannan, 2012; Morgan J. Hurley et al., 2016) and fuzzy possibility theory (Liu and Liu, 2010; Men et al., 2022a; Qin et al., 2011; Zadeh, 1975) are stated in this section.

2.1. Earthquake-triggered fire domino scenarios

2.1.1. Historical accident analysis

Due to the flammable, explosive and toxic characteristics of various hazardous chemicals, CIPs can be regarded as typical accident-prone high-risk areas. Large-scale earthquakes can easily trigger a series of loss of containment (LOC) events in CIPs, causing massive fires (Misuri and Cozzani, 2021; Misuri et al., 2023). Statistical analysis of 79 earthquake-triggered Natech events (Krausmann et al., 2011) indicates that pipelines and storage tanks are particularly vulnerable to earthquake excitation. The release of hazardous materials can be observed in 73% of tank-related scenarios, with an ignition probability as high as 0.76, far exceeding the counterpart in technological accident scenarios. Statistical analysis results indicate that the most frequent technological hazards triggered by earthquakes are fires and hazardous materials release (without ignition).

More severely, the thermal radiation and the flame impingement generated by fires also caused severe damage to adjacent tanks, triggering subsequent domino accidents. Historical accidents indicate that E-FDSs are one of the most prone and dangerous multi-hazard coupling events in CIPs (Men et al., 2023b; Ricci et al., 2021). On August 17, 1999, a 7.4-magnitude earthquake occurred in Kocaeli, Turkey. As shown in Fig. 1, the earthquake triggered massive fires at the naphtha tank farm within the TUPRAS Izmit refinery, which started with four naphtha storage tanks. Then, fires spread through an open ditch to the tank farm located south towards the processing units, and two more naphtha tanks were engulfed by the flames and burned completely. As reported by (Cozzani et al., 2006), common fire types in chemical industries are pool fire, jet fire, fireball and flash fire. The escalation of fire domino accidents is mainly caused by thermal radiation and flame impingement.

2.1.2. Earthquake-fire coupling effects analysis

For the past few years, many scholars (Krishnan et al., 2023; Lou and Wang, 2022; Lou et al., 2023a; b) have gradually focused on the post-earthquake fire performance of various types of engineering structures. (Wang et al., 2020b) carried out a two-stage damage experiment procedure to investigate the post-earthquake fire performance of square concrete-filled steel tube columns. They found that the fire resistance of specimens is significantly affected by the degree of seismic damage. The more serious seismic damage results in less fire resistance time of concrete-filled steel tube columns. (Calayir et al., 2022) investigated the post-earthquake fire performance of fire door sets through an experimental cyclic and fire test program. Experimental results indicate that the fire resistance of post-earthquake damaged fire doors decreases by 70%. (Lou and Wang, 2022) designed a two-stage test procedure to investigate the mechanical properties of Q235 steel in post-earthquake fire scenarios. Experimental results indicate that the elastic modulus of Q235 specimens is obviously affected by the degree of seismic damage.

In fire scenarios, the tank shell temperature gradually increases due to the influence of flame impingement or thermal radiation. At the same time, the tank shell undergoes thermal expansion and the radial size of the tank wall increases. However, there are local high-temperature areas on the tank shell, and the thermal expansion is non-uniform, resulting in thermal stress inside the tank shell (Li et al., 2019; Liu et al., 2021). Under the combined action of thermal stress and thermal expansion, the radial displacement of the tank shell exhibits nonlinear characteristics, and sudden changes or cracks occur at a certain moment.

Geometric deformation caused by seismic damage alters the surface characteristics of its tank shell, thereby affecting the radiation absorption capacity of the shell surface. Distorted or displaced sections of the tank shell may be more exposed to direct flame contact, leading to localized hotspots and increased temperature gradients. The combination of thinning of the tank shell and the altered heat distribution can result in higher and more rapid temperature increases in the damaged regions compared to the undamaged sections of the tank. The temperature distribution of the deformed tank shell is more diffuse and non-uniform, which intensifies the generation of thermal stress inside the tank shell. Moreover, the seismic damage results in the generation of residual stress inside the storage tank. These residual stresses can affect the load-carrying capacity and deformation behavior of the tank under fire conditions.

The coupling effects between earthquake and fire lead to significant mutually amplified phenomena (Men et al., 2023b). The prior-acting seismic damage can have an impact on the load-carrying capacity, deformation behavior, and temperature distribution of SCTs under fire conditions, resulting in significant fire resistance attenuation of post-earthquake damaged SCTs (Girgin, 2011; Lou and Wang, 2022; Men et al., 2023a; Men et al., 2022b). As a result, the earthquake-fire coupling effects can significantly aggravate the escalation of domino accidents, leading to a non-linear risk superposition process. However, existing studies (Antonioni et al., 2007; Chen et al., 2023; Cozzani et al., 2014; Huang et al., 2020; Men et al., 2022b; Zeng et al., 2022) still adopt the traditional Probit model to model the evolution process of E-FDSs, ignoring the earthquake-fire coupling effects. Risk analysis results may

be underestimated without full consideration of the fire resistance attenuation caused by seismic damage, potentially leading to inadequate prevention & mitigation strategies. To the best of our knowledge, this is the first work on earthquake-fire coupling fragility analysis of SCTs.

2.2. Thermal response analysis

The historical fire accidents in CIPs demonstrate that the high-intensity heat load caused by fires may impose severe structural damage on cylindrical steel tanks. The potential failure modes mainly include bucking, cracking or rupture of containment, which may be caused by the decreased tensile strength of the tank wall, the increased internal pressure, the generated high local thermal stress, or the melting of the nonmetallic parts (Jia et al., 2017). Research on the thermal response behavior of SCT exposed to fires has received considerable attention in recent years. In this section, the pool-fire model (Mannan, 2012; Morgan J. Hurley et al., 2016) is first introduced. On this basis, a lumped temperature model (Jia et al., 2017) is given to model the temperature rise trend of the tank shell under the influence of flame impingement and thermal radiation, respectively. Due to the light-weight and generalization characteristics, the lumped temperature model can easily be introduced into the QRA framework.

2.2.1. Pool-fire Model

An empirical pool-fire model (Mannan, 2012; Morgan J. Hurley et al., 2016) is provided to calculate the flame height and the thermal radiation intensity. The flame height can be calculated as follows :

$$H_{\mathrm{pf}} = 42\left(\frac{m_{\mathrm{B}}}{\rho_{\mathrm{a}}\sqrt{gD_{\mathrm{pf}}}}\right)^{0.61} D_{\mathrm{pf}} \tag{1}$$

where H_{pf} is the flame height (windless condition), m; m_{B} is the combustion rate of flammable liquid, $\mathrm{kg \bullet m^{-2} \bullet s^{-1}}$; D_{pf} is the oil pool diameter, m; $\rho_{\mathrm{a}} = 1.2\mathrm{kg \bullet m^{-3}}$ is the air density; $g = 9.8\mathrm{m \bullet s^2}$ is the gravitational acceleration.

The solid flame model has been widely used to calculate the thermal radiation intensity of pool fires (Jia et al., 2017). The thermal radiation intensity can be calculated as follows (Mannan, 2012; Morgan J. Hurley et al., 2016).

$$\begin{cases}
I\left(x_{\mathrm{pf}}\right) = E_{\mathrm{pf}} F_{\mathrm{sv}} \tau_{\mathrm{a}} \ (2\text{–}1) \\
E_{\mathrm{pf}} = 140\mathrm{e}^{-0.12D_{\mathrm{pf}}} + 20\left(1 - \mathrm{e}^{-0.12D_{\mathrm{pf}}}\right) \ (2\text{–}2) \\
F_{\mathrm{sv}} = \left(F_{\mathrm{h}}^2 + F_{\mathrm{v}}^2\right)^{0.5} \ (2\text{–}3) \\
F_{\mathrm{h}} = \frac{1}{\pi}\left(\arctan\sqrt{\frac{x_{\mathrm{r}}+1}{x_{\mathrm{r}}-1}} - \frac{x_{\mathrm{r}}^2 - 1 + h_{\mathrm{r}}^2}{\sqrt{A_{\mathrm{r}}B_{\mathrm{r}}}}\arctan\sqrt{\frac{x_{\mathrm{r}}-1}{x_{\mathrm{r}}+1}\frac{A_{\mathrm{r}}}{B_{\mathrm{r}}}}\right) \ (2\text{–}4) \\
F_{\mathrm{v}} = \frac{1}{\pi}\left[\frac{1}{x_{\mathrm{r}}}\arctan\frac{h_{\mathrm{r}}}{\sqrt{x_{\mathrm{r}}^2-1}} + \frac{h_{\mathrm{r}}(A_{\mathrm{r}} - 2x_{\mathrm{r}})}{x_{\mathrm{r}}\sqrt{A_{\mathrm{r}}B_{\mathrm{r}}}}\arctan\sqrt{\frac{x_{\mathrm{r}}-1}{x_{\mathrm{r}}+1}\frac{A_{\mathrm{r}}}{B_{\mathrm{r}}}} - \frac{h_{\mathrm{r}}}{x_{\mathrm{r}}}\arctan\sqrt{\frac{x_{\mathrm{r}}-1}{x_{\mathrm{r}}+1}}\right] \ (2\text{–}5) \\
h_{\mathrm{r}} = 2H_{\mathrm{pf}}/D_{\mathrm{pf}} \ (2\text{–}6) \\
x_{\mathrm{r}} = \left(2x_{\mathrm{pf}} + D_{\mathrm{pf}}\right)/D_{\mathrm{pf}} \ (2\text{–}7) \\
A_{\mathrm{r}} = \left(x_{\mathrm{r}}+1\right)^2 + h_{\mathrm{r}}^2 \ (2\text{–}8) \\
B_{\mathrm{r}} = \left(x_{\mathrm{r}}-1\right)^2 + h_{\mathrm{r}}^2 \ (2\text{–}9) \\
\tau_{\mathrm{a}} = 2.02\left(p_{\mathrm{aw}}x_{\mathrm{pf}}\right)^{-0.09} \ (2\text{–}10) \\
p_{\mathrm{aw}} = 101325H_{\mathrm{ra}}e^{14.4114 - \frac{5328}{T_{\mathrm{a}}}} \ (2\text{–}11)
\end{cases}$$

where $I\left(x_{\mathrm{pf}}\right)$ is the thermal radiation intensity at distance x_{pf} from the flame, $\mathrm{W \bullet m^{-2}}$; x_{pf} is the distance between the flame and target, m; E_{pf} is the surface radiative heat flux of a cylindrical pool fire flame, $\mathrm{W \bullet m^{-2}}$; F_{sv} is the view factor of a solid flame model; τ_a is the atmospheric transmissivity. p_{aw} is the partial pressure of steam, $\mathrm{N \bullet m^{-2}}$; H_{ra} is the relative air humidity; $T_a = 293\mathrm{K}$ is the air temperature.

2.2.2. Lumped temperature model

Suppose that one side of the tank shell with infinite length and width is exposed to a stable fire directly. The increase in tank shell temperature is caused by the fire impingement. According to the lumped temperature model (Jia et al., 2017), the time-varying average temperature of the tank shell T_s can be formulated by the following differential equation.

$$c_w\rho_w h_w\frac{\mathrm{d}T_s}{\mathrm{d}t} = \left(\alpha_w\varepsilon_f\sigma T_f^4 - \varepsilon_w\sigma T_s^4\right) - \left(\varepsilon_w\sigma T_f^4 - \alpha_w\varepsilon_a\sigma T_a^4\right) \tag{3}$$

where c_w is the specific heat of the tank shell, $\mathrm{J{\cdot}kg^{-1}{\cdot}K^{-1}}$; ρ_w is the density of the tank material, $\mathrm{kg{\cdot}m^3}$; h_w is the thickness of the tank shell, m; α_w is the radiant surface absorptivity of the tank shell; ε_f is the radiant surface emissivity of the fire; $\sigma = 5.67 \times 10^{-8}\mathrm{W{\cdot}m^{-2}{\cdot}K^{-4}}$ is the Boltzmann constant; T_f is the temperature of the fire, K; ε_w is the emissivity of the tank shell; $\varepsilon_a = 0.9$ is the emissivity of air.

Formally, following the general form of the ordinary differential equation, the above Eq. (3) can be re-written as:

$$\frac{\mathrm{d}T_s}{\mathrm{d}t} = C_1T_s^4 + C_2\# \tag{4}$$

where $C_1 = -\frac{2\varepsilon_w\sigma}{c_w\rho_w h_w}$ and $C_2 = \frac{\alpha_w\varepsilon_f\sigma T_f^4 + \alpha_w\varepsilon_a\sigma T_a^4}{c_w\rho_w h_w}$ are two constants.

Assuming that the increase in tank shell temperature is caused by the fire thermal radiation, the lumped temperature model can be re-formulated as follows.

$$c_w\rho_w h_w\frac{\mathrm{d}T_s}{\mathrm{d}t} = \left(1000\alpha_w I - \varepsilon_w\sigma T_s^4\right) - \left(\varepsilon_w\sigma T_s^4 - \alpha_w\varepsilon_a\sigma T_a^4\right) \tag{5}$$

Similarly, the above Eq. (5) can be re-written as:

$$\frac{\mathrm{d}T_s}{\mathrm{d}t} = C_1T_s^4 + C_3 \tag{6}$$

where $C_3 = \frac{1000\alpha_w I + \alpha_w\varepsilon_a\sigma T_a^4}{c_w\rho_w h_w}$ is a constant.

Suppose that the initial value of the vertical plate $T_s(t=0) = T_a$, the Runge-Kutta method (Zwillinger, 1992) can be used to obtain the

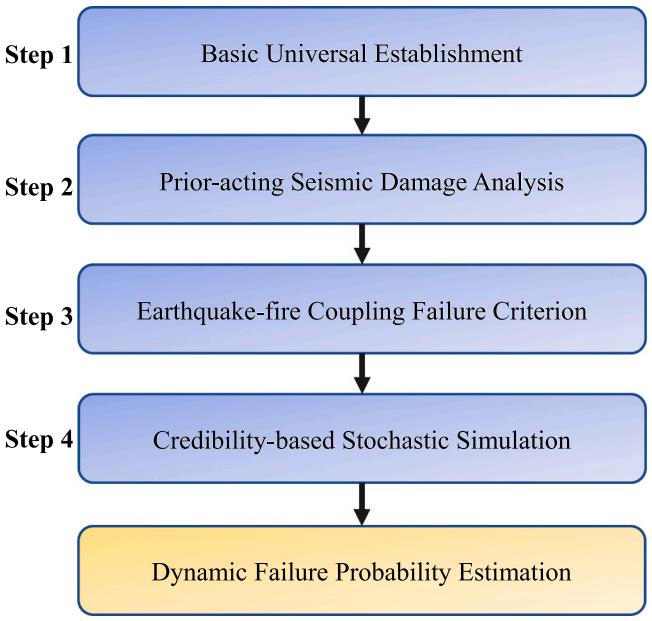

Fig. 2. The flowchart of the proposed methodology.

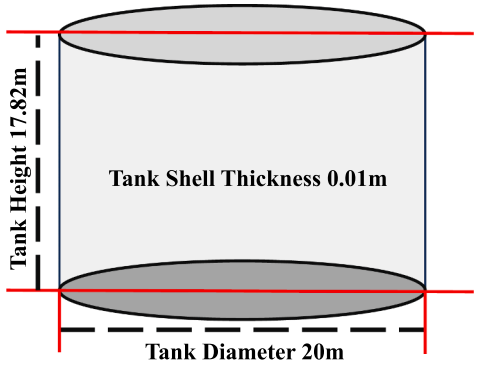

Fig. 3. Illustration of the 5000 m^3 fixed roof steel cylindrical tank.

temperature time curve of the tank shell.

2.3. Fuzzy possibility theory

In this section, some basic preliminaries about fuzzy possibility theory are stated to support the construction of multi-hazard coupling fragility analysis framework. To be specific, several crucial concepts in *possibility space*, *regular fuzzy variable* (R-FV), and *type 2 fuzzy variable* (T2-FV) are recalled. Related parameters are described in **Appendix. A**, **Table. A. 1**.

2.3.1. Possibility space

The triplet $(\Gamma, \mathscr{A}, Pos)$ is said to be a *possibility space* (Liu and Liu, 2010), of which Γ is denoted as the *universe*, $\mathscr{A}$ is the power set of Γ, and *Pos* is a *possibility measure*. For a specific problem, Γ can be regarded a non-empty set containing generic elements $\gamma \in \Gamma$, which should include all potential elements that might be involve (Qin et al., 2011). As the power set of Γ, $\mathscr{A}$ is a complete union of subsets of Γ. A *possibility measure Pos* is regarded as a set function $Pos: \mathscr{A} \to [0,1]$ that satisfies the following constraints (7–9) (Liu and Liu, 2010; Men et al., 2019).

$$Pos(\varnothing) = 0 \tag{7}$$

$$Pos(\Gamma) = 1 \tag{8}$$

For any subclass $\{A_i | i \in I\}$ of $\mathscr{A}$,

$$Pos(\cup_{i\in I} A_i) = Sup_{i\in I} A_i, \forall i \in I, \exists A_i \subset \mathscr{A} \tag{9}$$

According to the *possibility measure* $Pos(A)$, the *necessity measure* $Nec(A)$ and *credibility measure* $Cr(A)$ can be obtained as follows (Li, 2013):

$$Nec(A) = 1 - Pos(A^c) \tag{10}$$

$$Cr(A) = \frac{1}{2}(1 + Pos(A) - Pos(A^c)) \tag{11}$$

where $A \in \mathscr{A}$ is an element of $\mathscr{A}$, A^c is the complementary set of A.

2.3.2. Regular fuzzy variable

Suppose that the triplet $(\Gamma, \mathscr{A}, Pos)$ is a *possibility space*. A *fuzzy vector* $\boldsymbol{\xi} = (\xi_1, \xi_2, \ldots, \xi_m)$ is regarded as a m-dimension measurable map $\boldsymbol{\xi}: \Gamma \to \Re^m$, of which $\Re^m$ is a m-dimension real number space. For $\forall \boldsymbol{X} = (x_1, x_2, \ldots, x_m) \in \Re^m$, we have (Liu and Liu, 2010):

$$\{\gamma \in \Gamma | \boldsymbol{\xi}(\gamma) \le \boldsymbol{X}\} = \{\gamma \in \Gamma | \xi_1(\gamma) \le x_1, \ldots, \xi_m(\gamma) \le x_m\} \in \mathscr{A} \tag{12}$$

When $m = 1$ and $\Re = [0,1]$, ξ is denoted as a R-FV. The probability distribution function (PDF) of the R-FV is defined as follows (Liu and Liu, 2010):

$$\mu_\xi(x) = Pos(\{\gamma \in \Gamma | \xi(\gamma) = x\}), x \in [0,1] \tag{13}$$

Let $a, b, c, d \in [0,1]$ with $a < b < c < d$. A trapezoidal R-FV, denoted as $\xi = (a, b, c, d)$ is formulated by the following PDF:

$$\mu_\xi(x) = Pos\{\xi = x\} = \begin{cases} \dfrac{x-a}{b-a}, if \quad x \in [a,b] \\ 1, if \quad x \in (b,c) \\ \dfrac{d-x}{d-c}, if \quad x \in (c,d) \\ 0, otherwise \end{cases} \tag{14}$$

If $b = c$, then ξ is denoted as a triangular R-FV. Other common forms include the discrete R-FV, the Gaussian R-FV, and the like (Liu and Liu, 2010; Men et al., 2019; Qin et al., 2011; Zadeh, 1975).

2.3.3. Type 2 fuzzy variable

The exact PDF required by a R-FV is usually difficult to determine, since it depends on the data sources used and the assumptions made (Kundu et al., 2019; Men et al., 2019). To model the engineering application scenarios with more unknown information, type-2 fuzzy theory was proposed by (Zadeh, 1975), then (Liu and Liu, 2010) further extended the type-2 fuzzy theory to the *fuzzy probability space*. The T2-FV plays the same role in fuzzy possibility theory as a stochastic variable does in probability theory. The possibility of a T2-FV takes on a real number is an R-FV, which provides additional degrees of freedom for modeling uncertainties (Kundu et al., 2019; Men et al., 2019).

The triplet $(\Gamma, \mathscr{A}, \widetilde{Pos})$ is said to be a *fuzzy probability space*, of which $\widetilde{Pos}$ is a *fuzzy possibility measure*. Suppose that $\mathscr{R}([0,1])$ is the collection of all R-FVs on $[0,1]$. $\widetilde{Pos}$ is regarded as a set function $\widetilde{Pos}: \mathscr{A} \to \mathscr{R}([0,1])$ that satisfies the following two constraints (Liu and Liu, 2010; Men et al., 2019).

$$\widetilde{Pos}(\varnothing) = \widetilde{0} \tag{15}$$

$$\widetilde{Pos}(\cup_{i\in I} A_i) = Sup_{i\in I} \widetilde{Pos}\left(A_i\right), \forall i \in I, \exists A_i \subset \mathscr{A} \tag{16}$$

If $\mu_{\widetilde{Pos}(\Gamma)}(1) = 1$, then $\widetilde{Pos}$ is a *regular fuzzy possibility measure*. A *type 2 fuzzy vector* $\widetilde{\boldsymbol{\xi}} = (\widetilde{\xi}_1, \widetilde{\xi}_2, \ldots, \widetilde{\xi}_m)$ is regarded as a m-dimension measurable map $\widetilde{\boldsymbol{\xi}}: \Gamma \to \Re^m$, of which $\Re^m$ is a m-dimension real number space. For $\forall$

$\boldsymbol{X} = (x_1, x_2, \ldots, x_m) \in \Re^m$, we have (Liu and Liu, 2010):

$$\left\{\gamma \in \Gamma | \widetilde{\boldsymbol{\xi}}(\gamma) \le \boldsymbol{X}\right\} = \left\{\gamma \in \Gamma | \widetilde{\xi}_1(\gamma) \le x_1, \ldots, \widetilde{\xi}_m(\gamma) \le x_m\right\} \in \mathscr{A} \tag{17}$$

When $m = 1$, $\widetilde{\boldsymbol{\xi}}$ is denoted as a T2-FV. The secondary PDF of a T2-FV is a map $\Re \to \mathscr{R}([0,1])$, which is defined as follows (Li, 2013; Liu and Liu, 2010; Qin et al., 2011):

$$\widetilde{\mu}_{\widetilde{\xi}}(x) = \widetilde{Pos}\left\{\gamma \in \Gamma | \widetilde{\xi}(\gamma) = x\right\}, x \in \Re \tag{18}$$

The type-2 PDF of a T2-FV $\widetilde{\mu}_{\widetilde{\xi}}(x, \varphi)$ is regarded as the transformation of $\widetilde{Pos}$ from the universe Γ to the space $\Re$, i.e.$\Re \times J_x \to [0,1]$ (Li, 2013; Liu and Liu, 2010; Qin et al., 2011).

$$\widetilde{\mu}_{\widetilde{\xi}}(x, \varphi) = Pos\left\{\widetilde{\mu}_{\widetilde{\xi}}(x) = \varphi\right\}, J_x \subset [0,1], (x, \varphi) \in \Re \times J_x \tag{19}$$

where *Pos* is the possibility measure induced by the distribution of $\widetilde{\mu}_{\widetilde{\xi}}(x)$, $J_x = \left\{\varphi \in [0,1] | \widetilde{\mu}_{\widetilde{\xi}}(x, \varphi) > x\right\}$ is the primary membership of x.

3. Methodology

The flowchart of the proposed methodology is shown in Fig. 2, which consists of four main steps.

Step. 1 Basic Universal Establishment: A basic *universal* is established to express the knowledge about the coupling failure mechanism of SCTs in E-FDSs, which is the fundamental qualitative description of the fire resistance attenuation caused by seismic damage; **Step. 2 Prior-acting Seismic Damage Analysis:** Five seismic damage states of SCTs exposed to the ground motion caused by earthquakes are identified; **Step. 3 Earthquake-fire Coupling Failure Criterion:** A type-2 fuzzy time-dependent limit state equation is proposed to formulate the coupling failure criterion of SCTs subjected to the earthquake-fire sequence. The fire resistance attenuation caused by different seismic damage states is quantified by T2-FVs; **Step. 4 Credibility-based Stochastic Simulation:** Due to the fuzziness in probability distribution function, the type-2 fuzzy time-dependent limit state equation cannot be adopted for failure probability estimation directly (Liu and Liu, 2010; Men et al., 2022a; Qin et al., 2011). Following the critical value-based type reduction operation (CV-TR), T2-FVs are transformed into their corresponding R-FVs. After type reduction, the generalized credibility measure (Kundu et al., 2019; Li, 2013; Qin et al., 2011) is adopted to convert the type-2 fuzzy time-dependent limit state equation to its equivalent deterministic form. Finally, the dynamic failure probability estimation can be obtained by the stochastic simulation procedure.

3.1. Basic universal establishment

E-FDSs are one of the typical vicious cascading events associated with significant mutually amplified phenomena (Men et al., 2023b; Ricci et al., 2021). As mentioned in **Section 2.1** , numerical accident investigations (Girgin, 2011; Krausmann et al., 2011; Scawthorn and Johnson, 2000), simulations (Alasiri et al., 2021; Talebi et al., 2018; Vitorino et al., 2020) and experiments (Calayir et al., 2022; Lou and Wang, 2022; Wang et al., 2020b) were developed to investigate the post-earthquake fire performance of various engineering structures. The knowledge extracted from previous studies has provided strong evidence that the first-acting seismic excitation can weaken the ability of hazard-affected objects to resist subsequent fires. One of the toughest challenges in earthquake-fire coupling fragility analysis is quantifying the fire resistance attenuation caused by seismic damage. However, existing research and observations are still not enough to support parametric modeling. For the existing uncertainty analysis methodologies, the extracted knowledge is limited which is still not sufficient to support quantitative earthquake-fire coupling fragility analysis. Thus, according to the knowledge extracted from previous studies, a basic *universal* is established to qualitatively describe the fire resistance attenuation caused by the seismic damage, i.e. "*With other variables being the same, the failure probability of the SCT with serious prior-acting seismic damage is higher than the counterpart with light prior-acting seismic damage.*". The established universal is the core of the subsequent fragility analysis, which is adopted to guide the formulation of the post-earthquake fire failure criterion. The failure probability estimation must be consistent with the basic *universal*.

3.2. Prior-acting seismic damage analysis

SCTs constitute critical facilities of the chemical process industry. As mentioned by (Ozdemir et al., 2010), the seismic damage estimation of SCTs is a highly complex task due to the presence of various nonlinear behavior mechanisms in the fluid-structure interaction system. These mechanisms can be triggered simultaneously or independently, depending on multiple factors, such as seismic intensity, contained liquid properties and its depth, dimensions of the tank, material properties and supporting conditions and stiffness of underlying soil medium (Bakalis and Karamanos, 2021; Housner, 1957; Spritzer and Guzey, 2017).

The impulsive mass caused by seismic excitation may result in the tank shell buckling (Bakalis and Karamanos, 2021; Spritzer and Guzey, 2017). The elephant foot buckling and diamond-shaped buckling are the two most prominent buckling modes, as its characteristic elastoplastic outward bulging is formed as a result of the combined shell tensile hoop and compressive meridional stress (Bakalis and Karamanos, 2021; Spritzer and Guzey, 2017). Other potential failure modes include rupture of junction between tank shell and base, roof damage, tank support system and foundation failure and breaking of anchor bolts (Krausmann and Cruz, 2013; Miladi and S. Razzaghi, 2019; Ozdemir et al., 2010). Sloshing waves caused by the horizontal acceleration of the convective mass can also impose severe damage to tanks. The long-period dynamic forces due to the convective wave motion can damage the roof and cause the spilling of the tank contents.

Following the performance-based earthquake engineering framework (D'Amico and Buratti, 2018; Ghosh et al., 2021; Men et al., 2023a), damaged SCTs are typically classified into five damage states based on the severity of seismic damage, i.e. (1) No damage (DS_1: no damage to tank structure and accessories), (2) Minor damage (DS_2: damage to roof, minor loss of content, minor shell damage, minor piping damage, cracked foundation of the tank, no buckling), (3) Moderate damage (DS_3: buckling with no leak or minor loss of contents), (4) Severe damage (DS_4: buckling with major loss of contents, severe damage), (5) collapsed damage (DS_5: total failure, tank structure collapse). There is currently no unified and reliable structural damage index to quantify the seismic damage state. In real applications, the corresponding damage states are usually assigned to damaged tanks according to the qualitative descriptions of the seismic damage (D'Amico and Buratti, 2018; Men et al., 2023a; Wang et al., 2023).

Under this impetus, our previous study (Men et al., 2023a) proposed a hybrid deep belief network-based label distribution learning system to estimate the seismic damage state probability distribution of SCTs. According to the seismic response analysis, eight seismic damage parameters were adopted to characterize the seismic damage, i.e. (1) uplift force of tank bottom perimeter, (2) force resisting uplift in tank bottom, (3) force resisting uplift in annular region, (4) anchorage ratio, (5) maximum longitudinal shell compression stress, (6) hoop tensile stress, (7) allowable longitudinal shell-membrane compression stress, (8) sloshing wave height. Driven by a hybrid of post-earthquake damage data and seismic damage parameters, the proposed methodology can obtain the probability mapping relationship from physical damage characteristics to seismic damage states.

In this work, E-FDSs are of special concern, which aims to estimate the failure probability of post-earthquake damaged SCTs exposed to fire

with the consideration of the fire resistance attenuation caused by different seismic damage states. To avoid duplicating efforts from our previous study (Men et al., 2023a), the seismic damage states of SCTs are regarded as preconditions of the proposed time-dependent earthquake-fire coupling fragility analysis methodology.

3.3. Earthquake-fire coupling failure criterion

The damage to SCTs in fire scenarios is a time-dependent dynamic process (Cozzani et al., 2005; Lou and Wang, 2022). Therefore, unlike in seismic scenarios, the damage to SCTs in fire scenarios is not subdivided into distinct damage states, of which only operational and failed states are considered. In the early stages of domino effects research, the time to failure *ttf* is regarded as the failure threshold of SCTs in fire scenarios. As shown in Table 1, the calculation method *ttf* was fitted by (Cozzani et al., 2005) based on historical accident data. The failure of SCTs in fire scenarios is mainly caused by the decreased tensile strength of the tank wall, the increased internal pressure, the generated high local thermal stress, or the melting of the nonmetallic parts (Jia et al., 2017). Thus, (Jia et al., 2017) pointed out that the failure of SCTs is closely related to the tank shell temperature. The lumped temperature model was proposed to model the temperature rise trend of the tank shell under the influence of flame impingement and thermal radiation. The failure of SCTs requires a certain delay time, as the temperature of tank shell gradually rises to the critical temperature T_{cr} under the fire excitation (Lou and Wang, 2022). The critical temperature of steel was adopted to determine the state of SCTs (operational and failed). The critical temperature-based failure criterion has been widely used in subsequent studies (Ding et al., 2022; Li et al., 2023; Li et al., 2022; Li et al., 2019; Liu et al., 2021).

Suppose that t_{ef} is the fire exposure time (s), the fire failure criterion can be formulated by the following time-dependent limit state equation (Td-LSE):

$$\mathscr{L}_f(T_s, T_{cr}) = T_{cr} - T_s\left(t_{ef}\right) \tag{20}$$

where $T_s\left(t_{ef}\right)$ is the temperature of the tank shell with the fire exposure time t_{ef}. The value of $T_s\left(t_{ef}\right)$ can be obtained by solving the corresponding lumped temperature model (**Section 2.2**). $\mathscr{L}_f(T_s, T_{cr}) \geq 0$ indicates that the SCT is in the operational state; $\mathscr{L}_f(T_s, T_{cr}) < 0$ indicates that the SCT is in the failed state.

However, the above time-dependent LSE cannot capture the fire resistance attenuation caused by seismic damage. On the basis of critical temperature-based failure criterion and basic *universal*, the post-earthquake fire failure criterion can be formulated by the following type-2 fuzzy Td-LSE $\widetilde{\mathscr{L}}_{pef}$:

$$\begin{cases} \widetilde{\mathscr{L}}_{pef}\left(T_s, T_{cr}, \widetilde{\beta}^{DS_i}, \widetilde{\ell}\right) = \widetilde{\beta}^{DS_i} T_{cr} - \left(1 \pm \widetilde{\ell}\right) T_s\left(t_{ef}\right) \ (21\text{-}1) \\ \widetilde{0} < \widetilde{\beta}^{DS_i} \sim \widetilde{N}\left(\mu_1^{DS_i}, \left(\sigma_1^{DS_i}\right)^2; \theta_{l,1}^{DS_i}, \theta_{r,1}^{DS_i}\right) < \widetilde{\beta}^{DS_1} = \widetilde{1} \ (21\text{-}2) \\ \widetilde{0} < \widetilde{\ell} \sim \widetilde{N}\left(\mu_2, (\sigma_2)^2; \theta_{l,2}, \theta_{r,2}\right) \leq \widetilde{0.05} \ (21\text{-}3) \\ \widetilde{\beta}^{DS_1} > \widetilde{\beta}^{DS_2} > \widetilde{\beta}^{DS_3} > \widetilde{\beta}^{DS_4} \ (21\text{-}4) \end{cases}, i = 2, 3, 4$$

where the proposed type-2 fuzzy Td-LSE incorporates two kinds of T2-FVs $\widetilde{\beta}^{DS_i}$ and $\widetilde{\ell}$. $\widetilde{\beta}^{DS_i}$ is the type 2 fuzzy critical temperature attenuation coefficient derived from the *universal*. The fuzzy constraints $(21-2)$ and $(21-4)$ indicate that the more serious the damage state DS_i of a SCT, the lower its critical temperature $\widetilde{\beta}^{DS_i} T_{cr}$. $\widetilde{\ell}$ is the type 2 fuzzy deviation coefficient used to represent the temperature estimation deviation of the lumped temperature model. The fuzziness of the basic *universal* is represented by type 2 fuzzy variables. To guarantee the model universality, $\widetilde{\beta}^{DS_i}$ and $\widetilde{\ell}$ are assumed to be Gaussian T2-FVs with the following PDFs:

$$\widetilde{\mu}_{\widetilde{\beta}^{DS_i}}(x) = \left(G_1^{DS_i} - \theta_{l,1}^{DS_i} \min\left\{1 - G_1^{DS_i}, G_1^{DS_i}\right\}, G_1^{DS_i}, G_1^{DS_i} + \theta_{r,1}^{DS_i} \min\left\{1 - G_1^{DS_i}, G_1^{DS_i}\right\}\right) \tag{22}$$

$$\widetilde{\mu}_{\widetilde{\ell}}(x) = \left(G_2 - \theta_{l,2} \min\{1 - G_2, G_2\}, G_2, G_2 + \theta_{r,2} \min\{1 - G_2, G_2\}\right) \tag{23}$$

where $G_1^{DS_i} = \exp\left(-\frac{\left(x-\mu_1^{DS_i}\right)^2}{2\left(\sigma_1^{DS_i}\right)^2}\right)$, $G_2 = \exp\left(-\frac{(x-\mu_2)^2}{2(\sigma_2)^2}\right)$, x, $\mu_1^{DS_i}$, μ_2, $\sigma_1^{DS_i}$, $\sigma_2 \in \Re$; $\theta_l^{DS_i}, \theta_r^{DS_i}, \theta_{l,2}, \theta_{r,2}$ are the uncertainties that $\widetilde{\beta}^{DS_i}, \widetilde{\ell}$ takes the value of x. The advantage of using Gaussian T2-FVs for fragility analysis is that it allows for the consideration of a wider range of uncertainties and provides flexibility in handling the propagation and combination of uncertainties (Men et al., 2022a; Men et al., 2019; Xu et al., 2023). On the basis of prior observation extracted from experiments and numerical simulations, we have $\mu_1^{DS_2} = 0.910, \mu_1^{DS_3} = 0.779, \mu_1^{DS_4} = 0.672$. The confidence level of the lumped temperature model is assumed to be 95%, thus we have $\mu_2 = 0.05$.

It is worth mentioning that the fire resistance attenuation caused by seismic damage is not solely described by type 2 fuzzy variables. The precondition of $\widetilde{\beta}^{DS_i}$ is the seismic damage state of SCTs. According to our previous study (Men et al., 2023a), thirteen critical parameters affecting the seismic performance of SCTs were involved in the seismic damage analysis, i.e., (1) tank diameter, (2) tank height, (3) roof thicknesses, (4) shell thicknesses, (5) base thicknesses, (6) annular ring thicknesses, (7) roof type, (8) steel type, (9) anchorage system, (10) height of liquid level, (11) density of stored liquid, (12) peak ground acceleration, (13) soil classification. Moreover, as mentioned in **Section 2.1.2**, the temperature of the tank shell $T_s\left(t_{ef}\right)$ is crucial to identify the failure of SCTs. According to the lumped temperature model (**Section 2.2.2**), $T_s\left(t_{ef}\right)$ is closely related to the thermal radiation intensity, the temperature of the fire, the surface radiative heat flux of a cylindrical pool fire flame, the specific heat of the tank shell, the density of the tank material, the thickness of the tank shell, the radiant surface absorptivity of the tank shell, the radiant surface emissivity of the fire, the emissivity of the tank shell, etc. Thus, the established type-2 fuzzy Td-LSE actually considers the influence of multiple critical parameters.

3.4. Credibility-based stochastic simulation

In this section, a credibility-based stochastic simulation algorithm (C-SSA) is proposed to analyze the uncertainties in type 2 *fuzzy probability space*. The pseudo-code of the proposed C-SSA is shown in Algorithm 1. As mentioned in **Section 2.2**, the Runge-Kutta method (Zwillinger, 1992) is adopted for thermal response analysis, thus, $T_s\left(t_{ef}\right)$ can be obtained. The secondary PDFs of $\widetilde{\beta}^{DS_i}$ and $\widetilde{\ell}$ are

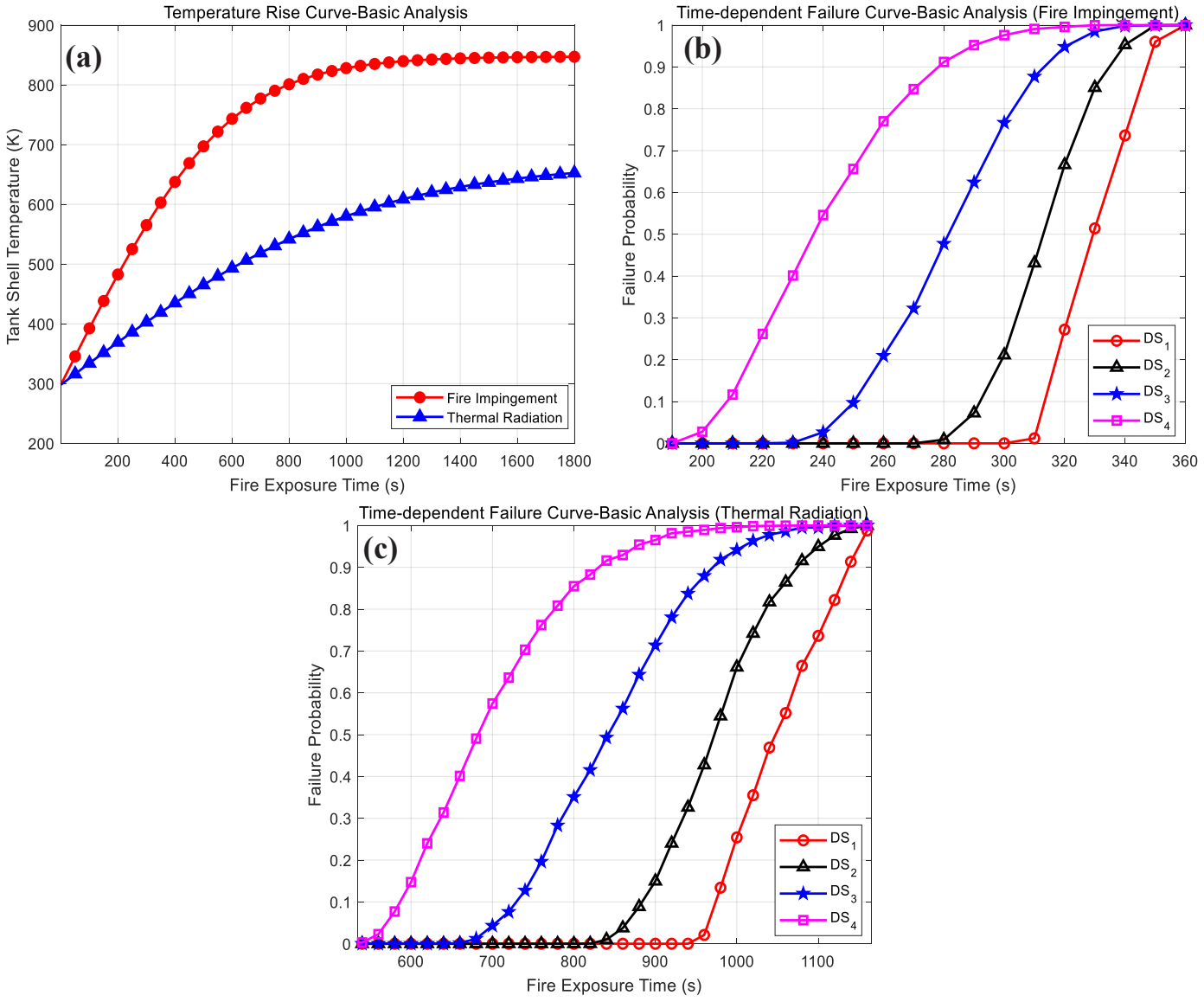

Fig. 4. Results of basic analysis, (a) Temperature Rise Curves; (b) Fire Impingement; (c) Thermal Radiation.

Table 2
Time-dependent failure probabilities of seismic damaged SCTs exposed to the fire impingement.

t_{ef}, s	$Ts(t_{ef})$, K	Failure Probability			
		DS_1	DS_2	DS_3	DS_4
195	4.782e+ 02	0	0	0	7.000e-03
230	5.083e+ 02	0	0	1.600e-03	4.012e-01
280	5.495e+ 02	0	8.800e-03	4.774e-01	9.118e-01
310	5.731e+ 02	1.200e-02	4.310e-01	8.770e-01	9.908e-01
335	5.919e+ 02	6.282e-01	9.064e-01	9.916e-01	1.000
350	6.029e+ 02	9.602e-01	9.992e-01	1.000	1.000
355	6.065e+ 02	1.000	1.000	1.000	1.000

Table 3
Time-dependent failure probabilities of seismic damaged SCTs exposed to the thermal radiation.

t_{ef}, s	$Ts(t_{ef})$, K	Failure Probability			
		DS_1	DS_2	DS_3	DS_4
535	4.753e+ 02	0	0	0	6.000e-04
655	5.076e+ 02	0	0	6.000e-04	3.898e-01
820	5.461e+ 02	0	2.000e-04	4.156e-01	8.826e-01
960	5.733e+ 02	2.100e-02	4.274e-01	8.794e-01	9.894e-01
1050	5.881e+ 02	5.168e-01	8.454e-01	9.864e-01	1.000
1145	6.017e+ 02	9.260e-01	9.978e-01	1.000	1.000
1160	6.037e+ 02	9.880e-01	1.000	1.000	1.000
1165	6.044e+ 02	1.000	1.000	1.000	1.000

formulated by the corresponding random parameter combinations ($\theta_{l,1}^{DS_i}$, $\theta_{r,1}^{DS_i}$, $\sigma_1^{DS_i}$) and ($\theta_{l,2}, \theta_{r,2}, \sigma_2$). The Monte Carlo random simulation method under a standard normal distribution is used to obtain random combinations of parameters. According to the basic *universal*, the critical temperature attenuation coefficients of different prior-acting seismic damage states are required to satisfy the constraints (21−2). Given the type 2 fuzziness involved in $\widetilde{\mathscr{L}}_{pef}$, CV-TR (Qin et al., 2011) is

implemented to convert $\widetilde{\beta}^{DS_i}$ to the corresponding R-FVs. Then, the credibility measure is adopted to obtain the equivalent deterministic LSE $\mathscr{L}_{pef}$. After a certain number of stochastic simulations, the failure probability estimation $p_f = \frac{N_f}{N_s}$ can be obtained.

Algorithm 1. Credibility-based Stochastic Simulation Algorithm.

Input:
The number of simulations N_s; Instance parameter set I_s;
Prior-acting seismic damage state DS_i; The time of a SCT exposed to fire t_{ef};
Output: Failure probability p_f
Initialize: $n = 0;\ N_f = 0$
While $n \le N_s$ ***Do***
  Thermal Response Analysis: $T_s(t_{ef}) \leftarrow LTM$
  Monte Carlo Sampling: $(\theta_{l,1}^{DS_i}, \theta_{r,1}^{DS_i}, \sigma_1^{DS_i}, \theta_{l,2}, \theta_{r,2}, \sigma_2, \varphi) \leftarrow MCS$
  Type Reduction: $\beta^{DS_i}, \ell \leftarrow CV(\widetilde{\beta}^{DS_i}, \widetilde{\ell})$
  Defuzzification: $\mathcal{L}_{pef} \leftarrow CM(\tilde{\mathcal{L}}_{pef})$
  If $\mathcal{L}_{pef} < 0$ ***Do***
    $N_f = N_f + 1$
  End If
End While
Failure probability Estimation: $p_f = \frac{N_f}{N_s}$

3.4.1. Type Reduction

The type-2 fuzzy LSE $\widetilde{\mathscr{L}}_{pef}$ provides additional degrees of freedom for modeling uncertainties, which also brings high computational complexity (Men et al., 2019). To handle the type-2 fuzziness, the CV-TR (Qin et al., 2011) is implemented to convert $\widetilde{\beta}^{DS_i} \sim \widetilde{N}(\ \mu^{DS_i}, (\sigma^{DS_i})^2; \theta_l^{DS_i}, \theta_r^{DS_i})$ and $\widetilde{\ell} \sim \widetilde{N}(\ \mu_2, (\sigma_2\ )^2; \theta_{l,2}, \theta_{r,2})$ to the following R-FV β^{DS_i} and ℓ.

$$\mu_{\beta^{DS_i}}(x) = \begin{cases} \dfrac{\left(1+\theta_{r,1}^{DS_i}\right)G_1^{DS_i}}{1+2\theta_{r,1}^{DS_i}G_1^{DS_i}}, if\ \ x \le \mu_1^{DS_i} - \sigma_1^{DS_i}\sqrt{2\ln 2}\ \ or\ \ x \ge \mu_1^{DS_i} + \sigma_1^{DS_i}\sqrt{2\ln 2} \\ \dfrac{\theta_{l,1}^{DS_i} + \left(1-\theta_{l,1}^{DS_i}\right)G_1^{DS_i}}{1+2\theta_{l,1}^{DS_i} - 2\theta_{l,1}^{DS_i}G_1^{DS_i}}, if\ \ \mu_1^{DS_i} - \sigma_1^{DS_i}\sqrt{2\ln 2} < x < \mu_1^{DS_i} + \sigma_1^{DS_i}\sqrt{2\ln 2} \end{cases} \tag{24}$$

$$\mu_{\ell}(x) = \begin{cases} \dfrac{(1+\theta_{r,2})G_2}{1+2\theta_{r,2}G_2}, if\ \ \ x \le \mu_2 - \sigma_2\sqrt{2\ln 2}\ \ \ or\ \ \ x \ge \mu_2 + \sigma_2\sqrt{2\ln 2} \\ \dfrac{\theta_{l,2}^{DS_i} + \left(1-\theta_{l,2}^{DS_i}\right)G_2^{DS_i}}{1+2\theta_{l,2}^{DS_i} - 2\theta_{l,2}^{DS_i}G_2^{DS_i}}, if\ \ \ \mu_2 - \sigma_2\sqrt{2\ln 2} < x < \mu_2 + \sigma_2\sqrt{2\ln 2} \end{cases} \tag{25}$$

Theoretical proof and detailed formula derivation of the type reduction process can be found in **Appendix. B**. An illustration of the type reduction process is stated in **Appendix. C**.

3.4.2. Defuzzification

After type reduction, the generalized credibility measure (Kundu et al., 2019; Li, 2013; Qin et al., 2011) is adopted to convert the original uncertainty model into its equivalent deterministic form. In this work, the failure of a SCT in E-FDSs is regarded as a fuzzy event $\left\{\widetilde{\beta}^{DS_i} T_{cr} - (1 \pm \widetilde{\ell}) T_s(t_{ef}) < 0\right\}$. Given the pre-defined credibility level, we have the following equivalent deterministic Td-LSE $\widetilde{Cr}\{\mathscr{L}_{pef} < 0\}$.

$$Cr\{\mathscr{L}_{pef} < 0\} \rightarrow T_{cr}E_d^1 - \left(1 \pm E_d^2\right)T_s\left(t_{ef}\right) < 0 \tag{26}$$

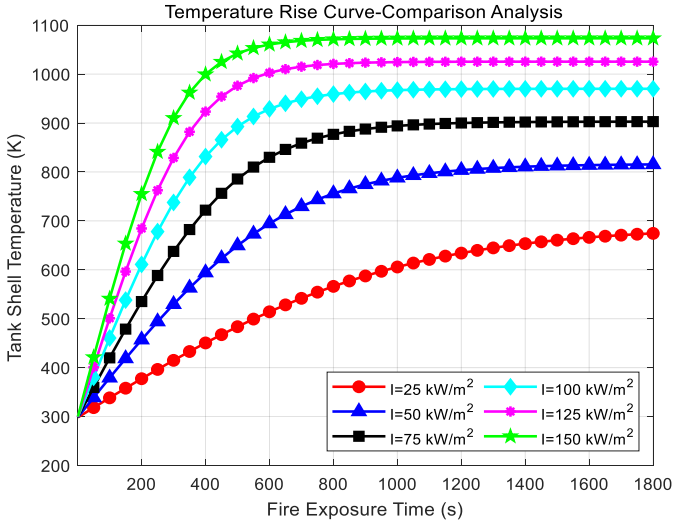

Fig. 5. Temperature Rise Curves-Comparison analysis.

Table 4
Results obtained by the Probit model.

I, kW • m^{-2}	ttf, s	$Ts(ttf)$, K	$P_{probit}(I)$
50	2.066e+02	4.608e+02	5.953e-03
75	1.308e+02	4.554e+02	4.059e-02
100	9.453e+01	4.526e+02	1.096e-01
125	7.350e+01	4.512e+02	1.950e-01
150	5.984e+01	4.456e+02	2.782e-01

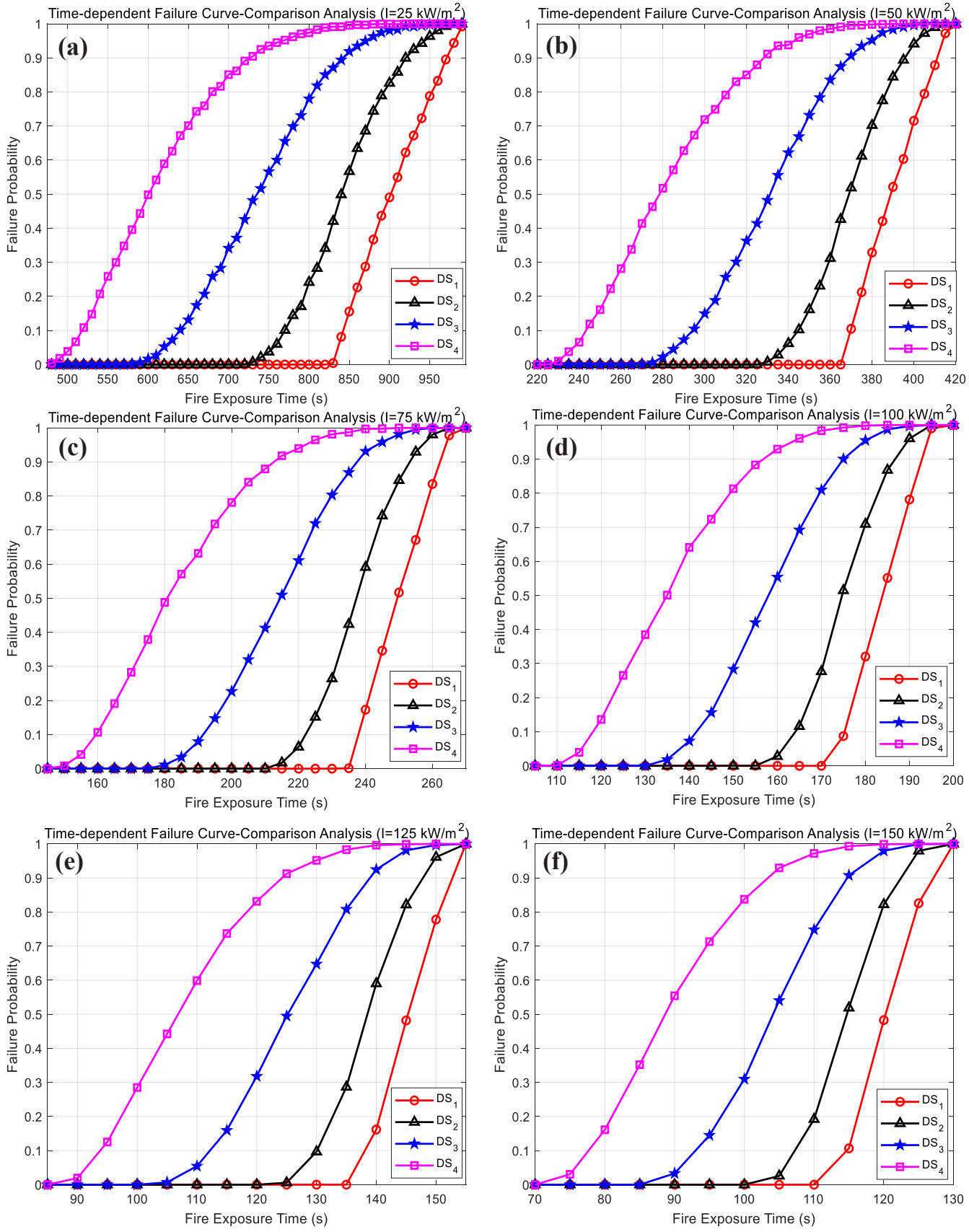

Fig. 6. Time-dependent Failure Probability Curves-Comparison Analysis, (a) $I = 25\text{kW} \bullet \text{m}^{-2}$; (b) $I = 50\text{kW} \bullet \text{m}^{-2}$; (c) $I = 75\text{kW} \bullet \text{m}^{-2}$; (d) $I = 100\text{kW} \bullet \text{m}^{-2}$; (e) $I = 125\text{kW} \bullet \text{m}^{-2}$; (f) $I = 150\text{kW} \bullet \text{m}^{-2}$.

$$E_d^1 = \begin{cases} \mu_1^{DS_i} - \sigma_1^{DS_i}\sqrt{2ln\left(1+(1-4\varphi)\theta_{r,1}^{DS_i}\right) - 2ln2\varphi}, \varphi \in \left(0, 0.25\right] \\ \mu_1^{DS_i} - \sigma_1^{DS_i}\sqrt{2ln\left(1+\left(4\varphi-1\right)\theta_{l,1}^{DS_i}\right) - 2ln\left(2\varphi+\left(4\varphi-1\right)\theta_{l,1}^{DS_i}\right)} \varphi \in (0.25] \\ \mu_1^{DS_i} + \sigma_1^{DS_i}\sqrt{2ln\left(1+\left(3-4\varphi\right)\theta_{l,1}^{DS_i}\right) - 2ln2\left(1-\varphi\right) + \left(3-4\varphi\right)\theta_{l,1}^{DS_i}\right)}, \varphi \in \left(0.5, 0.75\right] \\ \mu_1^{DS_i} + \sigma_1^{DS_i}\sqrt{2ln\left(1+\left(4\varphi-3\right)\theta_{r,1}^{DS_i}\right) - 2ln2\left(1-\varphi\right)}\varphi, \varphi\theta\left(0.75, 1\right] \end{cases} \tag{27}$$

$$E_d^2 = \begin{cases} \mu_2 - \sigma_2\sqrt{2\ln\left(1+(1-4\varphi)\theta_{r,2}\right) - 2\ln2\varphi}, \varphi \in (0, 0.25) \\ \mu_2 - \sigma_2\sqrt{2\ln\left(1+(4\varphi-1)\theta_{l,2}\right) - 2\ln\left(2\varphi+(4\varphi-1)\theta_{l,2}\right)}, \varphi \in (0.25, 0.5) \\ \mu_2 + \sigma_2\sqrt{2\ln\left(1+(3-4\varphi)\theta_{l,2}\right) - 2\ln2(1-\varphi) + (3-4\varphi)\theta_{l,2}} \quad, \varphi \in (0.5, 0.75) \\ \mu_2 + \sigma_2\sqrt{2\ln\left(1+(4\varphi-3)\theta_{r,2}\right) - 2\ln2(1-\varphi)}, \varphi \in (0.75, 1) \end{cases} \tag{28}$$

Theoretical proof and detailed formula derivation of the defuzzification process can be found in **Appendix. D**. According to the above equivalent deterministic failure criterion Td-LSE, the state of the SCT (operational and failed) can be determined.

4. Case studies

4.1. Instance description

To demonstrate the proposed methodology, a 5000 m^3 fixed roof SCT (Tank Diameter 20 m, Tank Height 17.82 m, and Tank Shell Thickness 0.01 m) is selected for case studies. The 5000 m^3 fixed roof SCT is designed based on the Chinese Standard (GB1, 0341–, 2014), which has been widely used for fire resistance performance analysis (Huang et al., 2023; Li et al., 2023; Li et al., 2019). In practical applications, our previous study (Men et al., 2023a) can be used for seismic damage estimation. An illustration of the seismic damage estimation is shown in **Appendix. E**. In this work, the fire resistance attenuation caused by different seismic damage states is of special concern. To avoid duplicating efforts, in this work, the seismic damage states of the 5000 m^3 fixed roof SCT are regarded as preconditions.

The specific heat of the tank shell $c_w = 460J{\cdot}kg^{-1}{\cdot}K^{-1}$; the density of the tank material $\rho_w = 7850kg{\cdot}m^3$; the radiant surface absorptivity of the tank shell $\alpha_w = 0.7$; the emissivity of the tank shell $\varepsilon_w = 0.35$. It is assumed that an earthquake triggered a pool fire (oil pool diameter $D_{pf} = 10m$) in the tank farm. As mentioned in **Section 2.1.1** , two common fire domino escalation scenarios are considered, i.e., the near-field pool fire scenario (flame impingement) and the far-field pool fire scenario (thermal radiation). The radiant surface emissivity of the fire $\varepsilon_f = 0.7$ and the temperature of the fire $T_f = 1100$. For the far-field pool fire scenario, the distance between the flame and target $x_{pf} = 5m$. By inputting the given parameters into the empirical pool-fire model (Mannan, 2012; Morgan J. Hurley et al., 2016), the thermal radiation intensity at the target location can be calculated as $22.449kW \bullet m^{-2}$. According to the previous analysis provided by (Li et al., 2019), the basic critical temperature $T_{cr} = 587.67K$. The number of simulations $N_s = 5,000$.

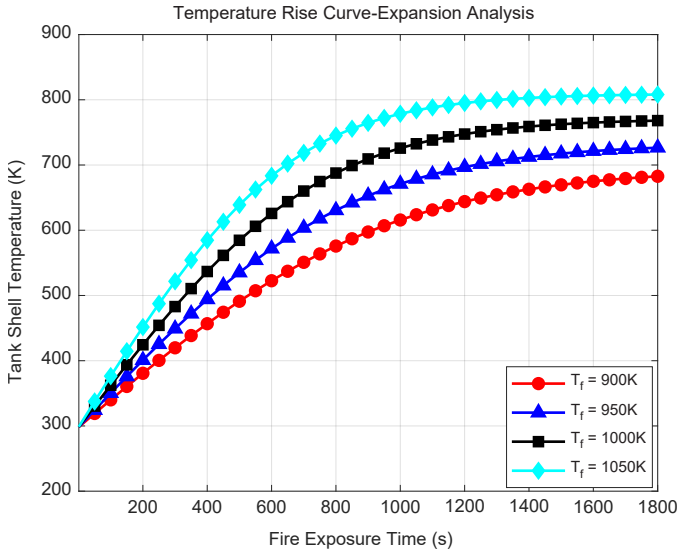

Fig. 7. Temperature Rise Curves- Expansion analysis.

4.2. Basic analysis

The temperature rise curves under the two fire scenarios can be seen in Fig. 4(a). When the SCT is exposed to a fire, the increase in tank shell temperature involves multiple heat transfer processes, including thermal radiation, heat conduction, and convective heat transfer (Li et al., 2023; Li et al., 2019).

For the scenario where the flame directly contacts the tank shell (near-field pool fire scenario), the heat transfer process is dominated by heat conduction, and the maximum temperature of the tank shell is 8.470e+ 02 K. For the far-field pool fire scenario, the heat transfer process is dominated by thermal radiation, and the maximum temperature of the tank shell is 6.528e+ 02 K. As shown in Fig. 4(a), the temperature rise caused by flame impingement is significantly faster.

According to the traditional *Probit* model (shown in Table 1), the *ttf* of the 5000 m^3 SCTs under the impact of 22.449 $kW \bullet m^{-2}$ thermal radiation is 5.098e + 02s. As shown in Fig. 4(c), at a fire exposure time of 5.098e+ 02 s, the failure probabilities of SCTs under different seismic damage states are 0. The corresponding Probit-based failure probability is 1.990e-05, which can also be approximated as 0. This indicates that the failure probability estimation obtained by the proposed methodology is to some extent consistent with the historical accident data-driven Probit model. However, as the thermal radiation continues to exert its effect, the failure probabilities of SCTs gradually increase. Static methods fail to capture the subsequent dynamic increase in failure probability, thereby limiting their ability to accurately assess the evolving risk.

The time-dependent failure probabilities of seismic damaged SCTs are shown in Table 2 and Table 3. As shown in Fig. 4(b) and Table 2, with impacts of the flame impingement, the dynamic increase range of

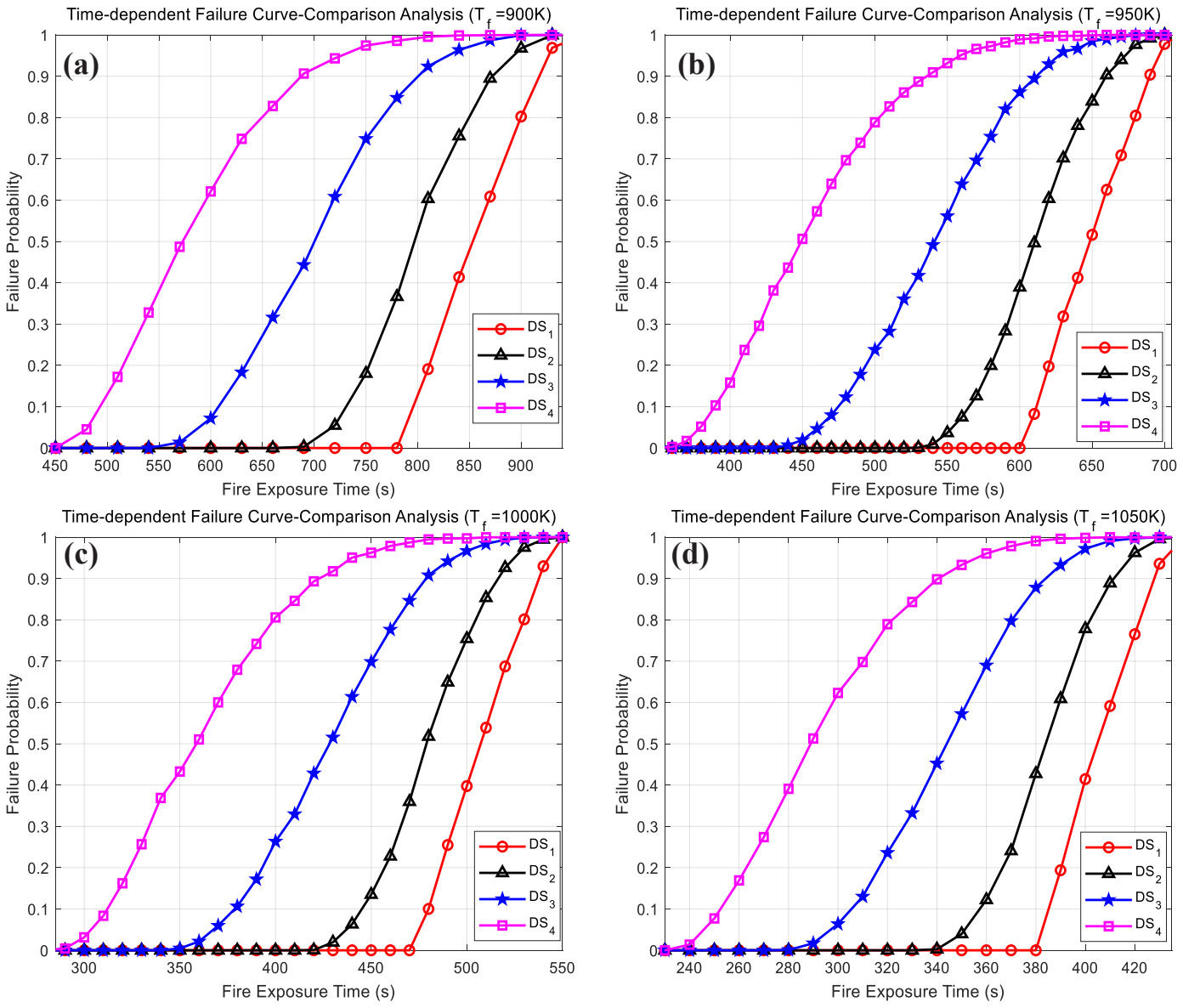

Fig. 8. Expansion analysis results, (a) $T_f = 900$K; (b) $T_f = 950$K; (c) $T_f = 1000$K; (d) $T_f = 1050$K.

the failure probability mainly concentrates from 195 s to 355 s of fire exposure time. As shown in Fig. 4(c) and Table 3, with impacts of the thermal radiation, the dynamic increase range of the failure probability mainly concentrates from 535 s to 1165 s of fire exposure time. Compared to the far-field pool fire scenario, SCTs are more prone to rapid failure under the impact of flame impingement. In actual chemical tank farms, multiple tanks may be located within the same containment area. When a flammable substance leak ignites, adjacent tanks are highly susceptible to being engulfed by the surrounding flames, which can further escalate the probability of domino effect accidents.

In addition, it can be observed that there are significant differences in the failure probabilities of the SCTs in different seismic damage states. Suppose that $p_f(DS_i, tef)$ is the time-dependent failure probability of the SCTs in seismic damage state DS_i, we have $p_f(DS_4, tef) \geq p_f(DS_3, tef) \geq p_f(DS_2, tef) \geq p_f(DS_1, tef)$. The failure probability estimation results are consistent with the basic *universal*. As the fire exposure time and the tank shell temperature increase, the differences in failure probabilities gradually increase and eventually converge or become consistent. As shown in Table 2, for SCTs exposed to the fire impingement, the impact of seismic damage on failure probabilities is most significant within the fire exposure time range from 230 s to 335 s, and the corresponding temperature range is from 5.083e+ 02 to 5.919e+ 02. As shown in Table 3, for SCTs exposed to thermal radiation, the impact of seismic damage on failure probabilities is most significant within the fire exposure time range from 655 s to 1050 s, and the corresponding temperature range is from 5.076e+ 02 to 5.881e+ 02. The proposed methodology can effectively estimate the time-dependent fire failure probability of SCTs with different seismic damage severities.

4.3. Comparison analysis

To further demonstrate the advantages of the proposed method, a comparison analysis is constructed between the proposed methodology and the Probit model. Temperature rise curves under different thermal radiation intensities (25, 50, 75, 100, 125, 150 kW • m^{-2}) are shown in Fig. 5. It can be observed that the temperature rise rate and the maximum tank shell temperature increase with the increase of thermal radiation intensity. This is because the increase in radiation intensity results in more absorption of thermal radiation by the tank shell surface.

Suppose that $MaxT_s(I)$, K is the maximum tank shell temperature under the thermal radiation intensity I, kW • m^{-2}, we have $MaxT_s(25) =$

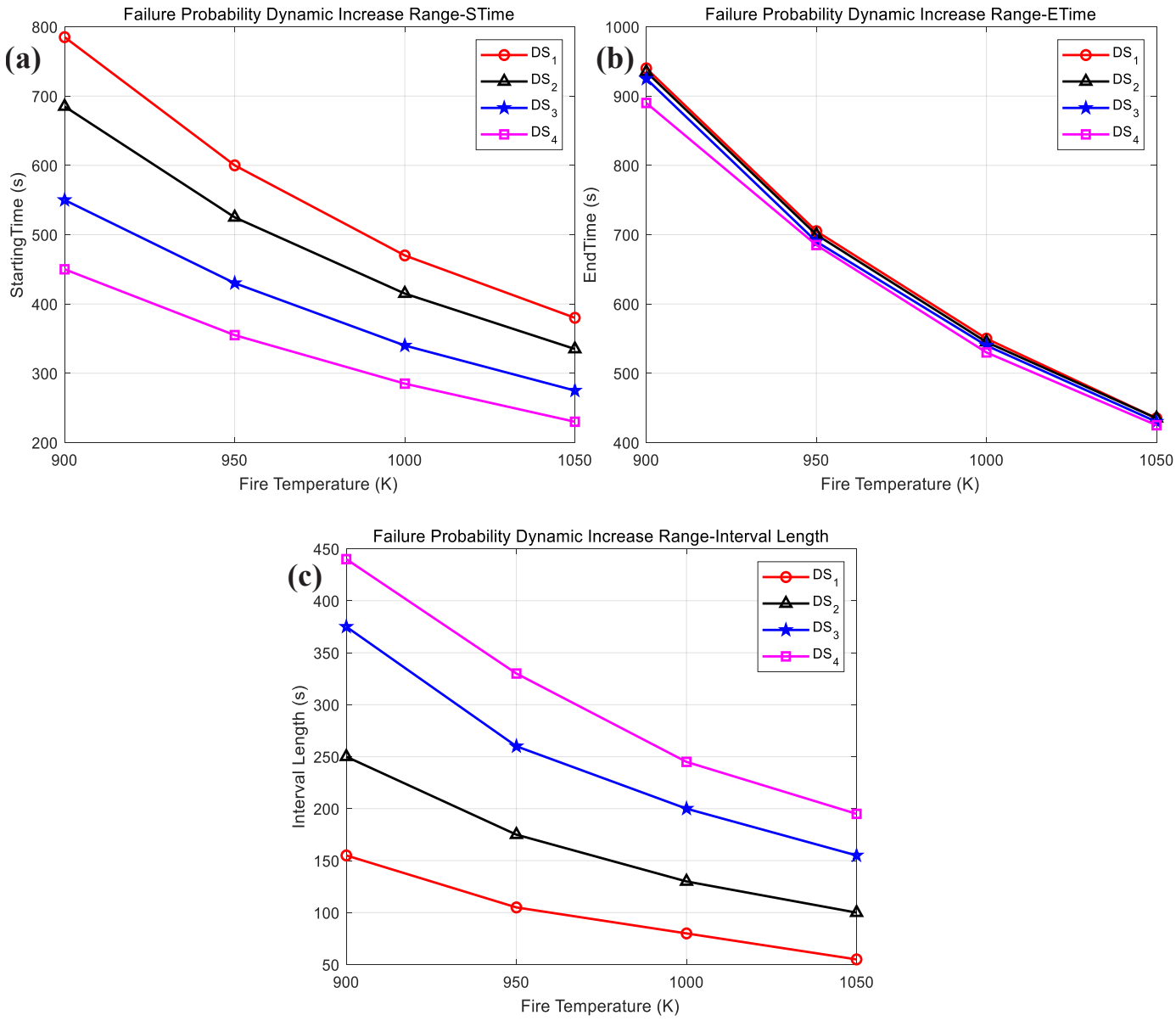

Fig. 9. Dynamic increase range of failure probability, (a) Start Times; (b) Termination Times; (c) Failure Interval.

6.746e + 02K, $MaxT_s(50)$ = 8.154e + 02K, $MaxT_s(75)$ = 9.029e + 02K, $MaxT_s(100)$ = 9.700e + 02K, $MaxT_s(125)$ = 1.025e + 03K, $MaxT_s(150)$ = 1.073e + 03K. In addition, we found that the thermal radiation intensity in the range of 25 kW • m^{-2} to 100 kW • m^{-2} has a more significant impact on the temperature rise trend of the tank shell.

Calculation results obtained by the Probit model are shown in Table 4. For thermal radiation intensities (25, 50, 75, 100, 125, 150 kW • m^{-2}), the corresponding *ttf* are 4.516e+ 02 s, 2.066e+ 02 s, 1.308e+ 02 s, 9.453e+ 01 s, 7.350e+ 01 s, 5.984e+ 01 s, respectively; the corresponding Probit-based failure probabilities are 4.983e-05, 5.953e-03, 4.059e-02, 1.096e-01, 1.950e-01, 2.782e-01, respectively. According to the lumped temperature model, the corresponding tank shell temperatures are 4.673e+ 02 K, 4.608e+ 02 K, 4.554e+ 02 K, 4.526e+ 02 K, 4.512e+ 02 K, 4.456e+ 02 K. Analysis results indicates that the values of *ttf* decrease with the increase of thermal radiation intensity. On the contrary, the Probit-based failure probabilities increase with the increase of heat radiation intensity.

The corresponding tank shell temperatures show little variation at the given *ttf* fire exposure time and remain relatively stable between 4.512e+ 02 K and 4.673e+ 02 K. This is a phenomenon that deserves great attention. This indicates a strong correlation between tank shell temperature and tank fire failure. The higher the thermal radiation intensity, the faster the rise in tank shell temperature, consequently leading to a decrease in *ttf*. As a data-driven failure probability estimation, the interpretability of the Probit model is not satisfactory. Through the lumped temperature model, the estimation results obtained by the Probit model can be explainable from the perspective of tank shell temperature.

However, as shown in Fig. 5, the temperature of the tank shell continues to increase even after reaching the *ttf* during fire exposure. The time-dependent failure probability curves obtained by the proposed methodology are shown in Fig. 6. Estimation results indicate that the ascending intervals of failure probabilities tend to advance with the increase of the thermal radiation intensity. In practical fire scenarios, the high temperature alters the crystalline structure of the tank shell, leading to a decrease in mechanical properties such as tensile strength, compressive strength, and yield strength. This can potentially result in tank deformation, cracking, leakage, and other forms of failure. Static probability estimation cannot capture the complex and dynamic failure process of SCTs in fire scenarios. Moreover, E-FDSs are usually

associated with significant mutually amplified phenomena, the first-acting seismic excitation can weaken the ability of SCTs to resist subsequent fires. Thus, the fire resistance attenuation caused by the seismic damage should be adequately considered when modeling the earthquake-triggered fire domino effects. Without the consideration of earthquake-fire coupling effects, the traditional Probit model is very likely to underestimate earthquake-triggered domino escalation probability. The proposed methodology can not only capture the fire resistance attenuation caused by seismic damage but also provide a dynamic estimation of tank failure probability with respect to the fire exposure time.

4.4. Expansion analysis

In this section, the influence of the fire temperature on the fire failure probability of post-earthquake damaged SCTs is analyzed. As shown in Fig. 7, under the impact of fire impingement, the rise rate of the tank shell temperature and the maximum tank shell temperature increase with the rise of the fire temperature T_f. The high-temperature flame makes the molecules on the tank wall surface more active, enhancing the efficiency of heat conduction. For fire temperatures $T_f = 900, 950, 1000, 1050, 1100$K, the corresponding maximum tank shell temperatures are 6.841e+ 02 K, 7.274e+ 02 K, 7.684e+ 02 K, 8.082e+ 02 K, 8.471e+ 02 K.

The corresponding time-dependent failure probability curves are shown in Fig. 8. It can be observed that the ascending intervals of failure probabilities differ significantly under different flame temperatures and seismic damage states. *Formally, the ascending interval of failure probability is defined as the dynamic fire failure interval.* As shown in Fig. 9, the dynamic increase range of failure probability is advanced with the increase of fire temperature. Additionally, we found that the starting time of the failure interval becomes shorter with increasing seismic damage severity. As the fire temperature increases, the difference in the failure intervals of SCTs under different seismic damage states gradually decreases. Similarly, as shown in Fig. 9(b), the termination times of the failure intervals for SCTs under different seismic damage states are very close. This is because the increase in fire temperature exacerbates the transition of tank shell temperature towards its steady-state peak value. The fire resistance attenuation caused by seismic damage is mainly manifested in the early and middle stages of the fire. In the later stages of the fire, the steady-state peak temperature of the tank shell far exceeds the critical temperature, and the influence of seismic damage on the failure probability becomes smaller. Compared to static fragility analysis, the proposed multi-hazard dynamic fragility analysis methodology can explicitly identify the dynamic fire failure interval of SCTs under different seismic damage states, rather than relying solely on a single *ttf* value.

5. Conclusions

In this work, an advanced multi-hazard dynamic fragility analysis methodology was proposed to cope with the prior knowledge and the dynamic evolution characteristics associated with earthquake-triggered fire domino effects. The fire resistance attenuation caused by seismic damage was qualitatively described by a basic *universal*. A type 2 fuzzy time-dependent limit state equation of steel cylindrical tanks exposed to earthquake-fire sequence was developed in which the uncertainties were modeled by Gaussian type 2 fuzzy variable. A credibility-based stochastic simulation algorithm is developed for the failure probability estimation in *fuzzy probability space*. Compared to the existing fragility analysis methods, the proposed methodology possesses enhanced capabilities in uncertainty modeling and analysis, achieving a hybrid uncertainty analysis that combines both ambiguity and stochasticity.

The proposed methodology was demonstrated by case studies of a 5000 m^3 fixed roof tank. Analysis results indicate that the proposed methodology can provide a reliable and explainable understanding of the evolving trends and differences in failure probability under different seismic damage states. The advantages of this work include high interpretability through seismic response analysis and thermal response analysis, the ability to capture the dynamic characteristics of the failure process, and the analysis of earthquake-fire coupling effects. The proposed can provide reliable and explainable probability estimation of earthquake-triggered fire domino escalation, which is the core for quantifying the dynamic risk evolution of earthquake-triggered fire domino scenarios. In practical applications, the obtained dynamic fire failure interval can also be used to guide emergency response planning.

Various catastrophic historical accidents demonstrate the importance of specifying efficient prevention & mitigation measures for multi-hazard coupling scenarios. Research on multi-hazard coupling scenarios is still in its infancy. There is still a need for a systematic and comprehensive quantitative risk assessment framework to integrate previous research. Moreover, detailed mechanism analysis is still required for more accurate probability estimation. These will also be focal points for our future work.

Declaration of Competing Interest

The authors declare the following financial interests/personal relationships which may be considered as potential competing interests: Guohua Chen reports financial support was provided by South China University of Technology.

Acknowledgements

This study was supported by the National Natural Science Foundation of China (22078109), the Key-Area Research and Development Program of Guangdong Province (2019B111102001), the China Scholarship Council (202206150061).

Appendix

A. Nomenclature.

B. Proof of Type Reduction Process.

Suppose that $\widetilde{\xi} \sim \widetilde{N}(\ \ \mu, \sigma^2; \theta_l, \theta_r)$ is a Gaussian T2-FV with secondary PDF $\widetilde{\mu}_{\widetilde{\xi}}(x)$.

$$\widetilde{\mu}_{\widetilde{\xi}}(x) = (G - \theta_l \min\{1-G, G\}, G, G + \theta_r \min\{1-G, G\}) \tag{B.1}$$

where $G = \exp\left(-\frac{(x-\mu)^2}{2\sigma^2}\right)$, $x, \mu \in \Re$, $\sigma > 0$. $\theta_l, \theta_r \in [0,1]$ are the uncertainty that $\widetilde{\xi}$ takes the value of x.

The critical value-based type reduction operation (Qin et al., 2011) can assign a crisp value to $\widetilde{\mu}_{\widetilde{\xi}}(x)$. $(G - \theta_l \min\{1-G, G\}, G, G + \theta_r \min\{1-G, G\})$

can be regarded as a triangular R-FV $\xi \sim (t_1,t_2,t_3)$, where $t_1 = G - \theta_l \min\{1-G, G\}$, $t_2 = G$, $t_3 = G + \theta_r \min\{1-G, G\}$. The PDF of triangular R-FV $\xi \sim (t_1, t_2, t_3)$ is defined as follows:

$$\mu_{\xi}(x) = \begin{cases} \dfrac{(x-t_1)}{t_2-t_1}, if \quad t_1 \le x < t_2 \\ 1, if \quad x = t_2 \\ \dfrac{t_3-x}{t_3-t_2}, if \quad t_2 < x \le t_3 \\ 0, otherwis \end{cases} \tag{B.2}$$

where $0 \le t_1 < t_2 < t_3 \le 1$. According to Eqs. (9), (10) and (11), we have:

$$Pos\{\xi \ge \varphi\} = \begin{cases} 1, if \quad \varphi \le t_2 \\ \dfrac{t_3-\varphi}{t_3-t_2}, if \quad t_2 < \varphi \le t_3 \\ 0, if \quad \varphi > t_3 \end{cases} \tag{B.3}$$

$$Nec\{\xi \ge \varphi\} = \begin{cases} 1, if \quad \varphi \le t_1 \\ \dfrac{t_2-\varphi}{t_2-t_1}, if \quad t_1 < \varphi \le t_2 \\ 0, if \quad \varphi > t_2 \end{cases} \tag{B.4}$$

$$Cr\{\xi \ge \varphi\} = \begin{cases} 1, if \quad \varphi \le t_1 \\ \dfrac{2t_2-t_1-\varphi}{2(t_2-t_1)}, if \quad t_1 < \varphi \le t_2 \\ \dfrac{t_3-\varphi}{2(t_3-t_2)}, if \quad t_2 < \varphi \le t_3 \\ 0, if \quad \varphi > t_3 \end{cases} \tag{B.5}$$

Following the critical value-based type reduction operation, the optimistic critical value of ξ is defined as follows

$$CV_{op}[\xi] = Sup_{\varphi\epsilon[0,1]}[\varphi \wedge Pos\{\xi \ge \varphi\}]$$

$$= Sup_{\varphi\epsilon[0,t_2]}[\varphi \wedge 1] \vee Sup_{\varphi\epsilon(t_2,t_3]}\left[\varphi \wedge \frac{t_3-\varphi}{t_3-t_2}\right] \vee Sup_{\varphi\epsilon(t_3,1]}[\varphi \wedge 0]$$

$$= \frac{t_3}{(1+t_3-t_2)} = \frac{G+\theta_r \min\{1-G, G\}}{(1+\theta_r \min\{1-G, G\})} \tag{B.6}$$

The pessimistic critical value of ξ is defined as follows:

$$CV_{pe}[\xi] = Sup_{\varphi\epsilon[0,1]}[\varphi \wedge Nec\{\xi \ge \varphi\}]$$

$$= Sup_{\varphi\epsilon[0,t_1]}[\varphi \wedge 1] \vee Sup_{\varphi\epsilon(t_1,t_2]}\left[\varphi \wedge \frac{t_2-\varphi}{t_2-t_1}\right] \vee Sup_{\varphi\epsilon(t_2,1]}[\varphi \wedge 0]$$

$$= \frac{t_2}{(1+t_2-t_1)} = \frac{G}{(1+\theta_l \min\{1-G, G\})} \tag{B.7}$$

The impartial critical value of ξ is defined as follows:

$$CV_{\mathrm{im}}[\xi] = Sup_{\varphi\epsilon[0,1]}[\varphi \wedge Cr\{\xi \ge \varphi\}]$$

$$= Sup_{\varphi\epsilon[0,t_1]}[\varphi \wedge 1] \vee Sup_{\varphi\epsilon(t_1,t_2]}\left[\varphi \wedge \frac{2t_2-t_1-\varphi}{2(t_2-t_1)}\right] \vee Sup_{\varphi\epsilon(t_2,t_3]}\left[\varphi \wedge \frac{t_3-\varphi}{2(t_3-t_2)}\right] \vee 0$$

$$= \begin{cases} \dfrac{2t_2-t_1}{1+2(t_2-t_1)} = \dfrac{G+\theta_l \min\{1-G, G\}}{1+2\theta_l \min\{1-G, G\}}, if \quad t_2 > \dfrac{1}{2} \\ \dfrac{2t_3}{1+2(t_3-t_2)} = \dfrac{2(G+\theta_r \min\{1-G, G\})}{1+2\theta_r \min\{1-G, G\}}, if \quad t_2 \le \dfrac{1}{2} \end{cases} \tag{B.8}$$

If $G \le 0.5$, then $\min\{1-G, G\} = G$. If $G > 0.5$, then $\min\{1-G, G\} = 1-G$. Thus, equations $(B.6)$, $(B.7)$ and $(B.8)$ are re-written as follows:

$$CV_{op}[\xi] = \begin{cases} \dfrac{(1+\theta_r)G}{1+\theta_r G}, if \quad x \le \mu - \sigma\sqrt{2\ln 2} \quad or \quad x \ge \mu + \sigma\sqrt{2\ln 2} \\ \dfrac{\theta_r + (1-\theta_r)G}{1+\theta_r - \theta_r G}, if \quad \mu - \sigma\sqrt{2\ln 2} < x < \mu + \sigma\sqrt{2\ln 2} \end{cases} \tag{B.9}$$

$$CV_{pe}[\xi] = \begin{cases} \dfrac{G}{1+\theta_l G}, if \quad x \le \mu - \sigma\sqrt{2\ln 2} \quad or \quad x \ge \mu + \sigma\sqrt{2\ln 2} \\ \dfrac{G}{1+\theta_l - \theta_l G}, if \quad \mu - \sigma\sqrt{2\ln 2} < x < \mu + \sigma\sqrt{2\ln 2} \end{cases} \tag{B.10}$$

$$CV_{\mathrm{im}}[\xi] = \begin{cases} \dfrac{(1+\theta_r)G}{1+2\theta_l G}, if \quad x \le \mu - \sigma\sqrt{2\ln 2} \quad or \quad x \ge \mu + \sigma\sqrt{2\ln 2} \\ \dfrac{\theta_l + (1-\theta_l)G}{1+2\theta_l - 2\theta_l G}, if \quad \mu - \sigma\sqrt{2\ln 2} < x < \mu + \sigma\sqrt{2\ln 2} \end{cases} \tag{B.11}$$

where $G \le 0.5 \Rightarrow \exp\left(-\frac{(x-\mu)^2}{2\sigma^2}\right) \le 0.5 \Rightarrow x \le \mu - \sigma\sqrt{2\ln 2} or\ x \ge \mu + \sigma\sqrt{2\ln 2}$ and $G > 0.5 \Rightarrow \exp\left(-\frac{(x-\mu)^2}{2\sigma^2}\right) > 0.5 \Rightarrow \mu - \sigma\sqrt{2\ln 2} < x < \mu + \sigma\sqrt{2\ln 2}$.

The reduction ξ of Gaussian T2-FV $\widetilde{\xi}$ is completed.

C. Illustration of the Type Reduction Process.

Suppose that $\widetilde{\xi} \sim \widetilde{N}(\ \ 0.5, 1; 0.3, 0.7)$ is a Gaussian T2-FV, ξ_{op}, ξ_{pe} and ξ_{im} are the optimistic, pessimistic, impartial reductions of $\widetilde{\xi}$.

$$G = \exp\left(-\frac{(x-\mu)^2}{2\sigma^2}\right) = \exp\left(-\frac{(x-0.5)^2}{2}\right) \tag{C.1}$$

According to equations $(B.9)$, $(B.10)$ and $(B.11)$, we have:

$$\mu_{\xi_{op}}(x) = \begin{cases} \dfrac{(1+0.7)G}{1+0.7G}, if \quad x \le 0.5 - \sqrt{2\ln 2} \quad or \quad x \ge 0.5 + \sqrt{2\ln 2} \\ \dfrac{0.7+0.3G}{1.7-0.7G}, if 0.5 - \sqrt{2\ln 2} < x < 0.5 + \sqrt{2\ln 2} \end{cases} \tag{C.2}$$

$$\mu_{\xi_{pe}}(x) = \begin{cases} \dfrac{G}{1+0.3G}, if \quad x \le 0.5 - \sqrt{2\ln 2} \quad or \quad x \ge 0.5 + \sqrt{2\ln 2} \\ \dfrac{G}{1.3-0.3G}, if 0.5 - \sqrt{2\ln 2} < x < 0.5 + \sqrt{2\ln 2} \end{cases} \tag{C.3}$$

$$\mu_{\xi_{\mathrm{im}}}(x) = \begin{cases} \dfrac{(1+0.7)G}{1+0.6G}, if \quad x \le 0.5 - \sqrt{2\ln 2} \quad or \quad x \ge 0.5 + \sqrt{2\ln 2} \\ \dfrac{0.7+0.3G}{1.6-0.6G}, if 0.5 - \sqrt{2\ln 2} < x < 0.5 + \sqrt{2\ln 2} \end{cases} \tag{C.4}$$

As shown in Fig. C. 1, through the critical value-based type reduction operation, Gaussian T2-FV $\widetilde{\xi}$ is transformed into three R-FVs ξ_{op}, ξ_{pe} and ξ_{im}. Generally, the impartial reduction ξ_{im} is widely-used for type reduction process (Liu and Liu, 2010; Men et al., 2022a; Qin et al., 2011).

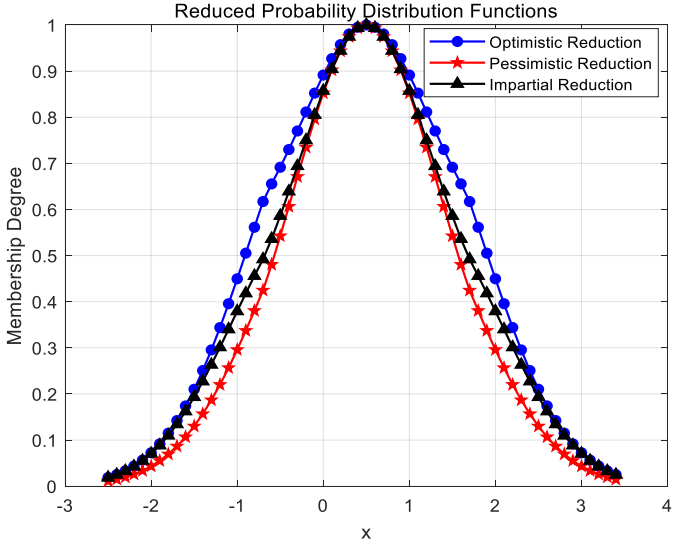

Fig. C. 1. Probability Distribution Functions of Three Reductions.

.

D. Proof of Defuzzification Process.

After type reduction, the generalized credibility measure (Kundu et al., 2019; Li, 2013; Qin et al., 2011) is adopted to convert the R-FV to its equivalent deterministic form. Suppose that ξ is the impartial reduction of a Gaussian T2-FV $\widetilde{\xi} \sim \widetilde{N}(\ \mu,\sigma^2;\theta_l,\theta_r)$, the generalized credibility measure of a fuzzy event $\{\xi \le \kappa\}$ can be defined as follows:

$$\widetilde{Cr}\{\xi \le \kappa\} = \frac{1}{2}\left(Sup_{x\in\Re}\mu_{\xi}(x) + Sup_{x\le\kappa}\mu_{\xi}(x) - Sup_{x>\kappa}\mu_{\xi}(x)\right) \tag{D.1}$$

where κ is deterministic variable. If $Cr\{\xi \ge \kappa\} + Cr\{\xi < \kappa\} = Sup_{x\in\Re}\mu_{\xi}(x) = 1$, then ξ is denoted as a normalized R-FV (Qin et al., 2011). Given the pre-defined credibility level $\varphi \in (0, 0.5]$, we have:

$$\widetilde{Cr}\{\xi \le \kappa\} = \frac{1}{2}\left(1 + Sup_{x\le\kappa}\mu_{\xi}(x) - 1\right) = \frac{1}{2}Sup_{x\le\kappa}\mu_{\xi}(x) \tag{D.2}$$

$$\widetilde{Cr}\{\xi \le \kappa\} \ge \varphi \Rightarrow Sup_{x\le\kappa}\mu_{\xi}(x) \ge 2\varphi \tag{D.3}$$

Following the definition of α-optimistic value (Liu and Liu, 2010; Qin et al., 2011), the α-optimistic value of ξ can be calculated as follows:

$$\xi_{\inf}(\alpha) = \inf\left\{\kappa | \widetilde{Cr}\{\xi \le \kappa\} \ge \alpha\right\}, \alpha\epsilon(0,1] \tag{D.4}$$

Suppose that $\alpha = 2\varphi$, we have:

$$\xi_{\inf}(2\varphi) \le \kappa \tag{D.5}$$

If $\varphi\epsilon(0, 0.25]$, $2\varphi \le 0.5$, $\xi_{\inf}(2\varphi)$ is the solution of $\frac{(1+\theta_r)G}{1+2\theta_l G} = 2\varphi$. If $\varphi\epsilon(0.25, 0.5]$, $2\varphi > 0.5$, $\xi_{\inf}(2\varphi)$ is the solution of $\frac{\theta_l+(1-\theta_l)G}{1+2\theta_l-2\theta_l G} = 2\varphi$. The analytical solutions are stated as follows:

$$\xi_{\inf}(2\varphi) = \begin{cases} \mu - \sigma\sqrt{2\ln(1+(1-4\varphi)\theta_r) - 2\ln 2\varphi}, if \quad \varphi\epsilon(0, 0.25) \\ \mu - \sigma\sqrt{2\ln(1+(4\varphi-1)\theta_r) - 2\ln(2\varphi+(4\varphi-1)\theta_l)}, if \quad \varphi\epsilon(0.25, 0.5) \end{cases} \tag{D.6}$$

Given the pre-defined credibility level $\varphi \in (0.5, 1]$, we have:

$$\widetilde{Cr}\{\xi \le \kappa\} = \frac{1}{2}\left(1 + 1 - Sup_{x>\kappa}\mu_{\xi}(x)\right) = 1 - \frac{1}{2}Sup_{x\le\kappa}\mu_{\xi}(x) \tag{D.7}$$

$$\widetilde{Cr}\{\xi \le \kappa\} \ge \varphi \Rightarrow Sup_{x\le\kappa}\mu_{\xi}(x) \ge 2 - 2\varphi \tag{D.8}$$

Suppose that $\alpha = 2 - 2\varphi$, we have:

$$\xi_{\inf}(2-2\varphi) \le \kappa \tag{D.9}$$

If $\varphi\epsilon(0.5, 0.75]$, $2-2\varphi > 0.5$, $\xi_{\inf}(2-2\varphi)$ is the solution of $\frac{\theta_l+(1-\theta_l)G}{1+2\theta_l-2\theta_l G} = 2 - 2\varphi$. If $\varphi\epsilon(0.75, 1]$, $2-2\alpha \le 0.5$, $\xi_{\inf}(2-2\varphi)$ is the solution of $\frac{(1+\theta_r)G}{1+2\theta_l G} = 2 - 2\varphi$. The analytical solutions are stated as follows:

$\xi_{\inf}(2-2\varphi) =$

$$\begin{cases} \mu + \sigma\sqrt{2\ln(1+(3-4\varphi)\theta_l) - 2\ln 2(1-\varphi) + (3-4\varphi)\theta_l}, if \quad \varphi\epsilon(0.5, 0.75) \\ \mu + \sigma\sqrt{2\ln(1+(4\varphi-3)\theta_r) - 2\ln 2(1-\varphi)}, if \quad \varphi\epsilon(0.75, 1) \end{cases} \tag{D.10}$$

To sum up, $\widetilde{Cr}\{\xi \le \kappa\} \ge \varphi$ is equivalent to:

$$\begin{cases} \mu - \sigma\sqrt{2\ln(1+(1-4\varphi)\theta_r) - 2\ln 2\varphi} \le \kappa, if \quad \varphi\epsilon(0, 0.25) \\ \mu - \sigma\sqrt{2\ln(1+(4\varphi-1)\theta_r) - 2\ln(2\varphi+(4\varphi-1)\theta_l)} \le \kappa, if \quad \varphi\epsilon(0.25, 0.5) \\ \mu + \sigma\sqrt{2\ln(1+(3-4\varphi)\theta_l) - 2\ln 2(1-\varphi) + (3-4\varphi)\theta_l}, if \quad \varphi\epsilon(0.5, 0.75) \\ \mu + \sigma\sqrt{2\ln(1+(4\varphi-3)\theta_r) - 2\ln 2(1-\varphi)}, if \quad \varphi\epsilon(0.75, 1) \end{cases} \tag{D.11}$$

The theoretical proof is complete.

E. Seismic Damage Estimation.

The proposed hybrid deep belief network-based label distribution learning system (Men et al., 2023a) is used to analyze the seismic damage state probability distribution of the 5000 m^3 fixed roof SCT under different seismic intensities (Peak Ground Acceleration). As shown in Fig. E. 1, seismic damage state probability curves were calculated for filling rates of 90%. The curves allow quantifying the likelihood of tank damage states under different seismic intensities. The damage state with highest probability is denoted as the dominant state of seismic damage. With the increase of Peak Ground Acceleration, the dominant state of seismic damage changes dynamically, exhibiting a clear trend of becoming more severe. In practical applications, this previous work (Men et al., 2023a) can provide preliminary analysis for earthquake-fire coupling fragility analysis.

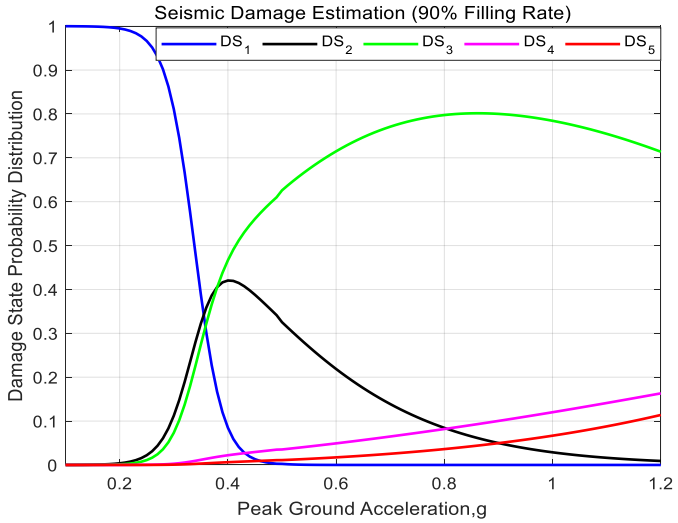

Fig. E. 1. Damage State Probability Distribution of the 5000 m^3 fixed roof SCT.

Table. A. 1
Notations for Fuzzy Possibility Theory.

Notations	Definitions
Γ	A non-empty set containing generic elements $\gamma \in \Gamma$
γ	Generic elements of Γ
$\mathscr{A}$	A complete union of subsets of Γ
Pos	*Possibility measure*
$(\Gamma, \mathscr{A}, Pos)$	*Possibility space*
Nec	*Necessity measure*
Cr	*Credibility measure*
$\boldsymbol{\xi}$	*Fuzzy vector,* a m-dimension measurable map $\boldsymbol{\xi} : \Gamma \rightarrow \Re^m$
$\Re^m$	A m-dimension real number space
$\mu_\xi(x)$	The probability distribution function of *regular fuzzy variable* ξ
$\widetilde{Pos}$	*Fuzzy possibility measure*
$(\Gamma, \mathscr{A}, \widetilde{Pos})$	*Fuzzy probability space*
$\widetilde{\boldsymbol{\xi}}$	*Type 2 fuzzy vector*
$\widetilde{\mu_{\tilde{\xi}}}(x)$	Secondary probability distribution function of type 2 fuzzy variable $\widetilde{\xi}$
J_x	The primary membership of x
φ	Pre-defined credibility level

References

Alasiri, M.R., Chicchi, R., Varma, A.H., 2021. Post-earthquake fire behavior and performance-based fire design of steel moment frame buildings. J. Constr. Steel Res. 177, 106442.

Antonioni, G., Spadoni, G., Cozzani, V., 2007. A methodology for the quantitative risk assessment of major accidents triggered by seismic events. J. Hazard. Mater. 147, 48–59.

Bai, M., Qi, M., Shu, C.-M., Reniers, G., Khan, F., Chen, C., Liu, Y., 2023. Why do major chemical accidents still happen in China: analysis from a process safety management perspective. Process Saf. Environ. Prot. 176, 411–420.

Bakalis, K., Karamanos, S.A., 2021. Uplift mechanics of unanchored liquid storage tanks subjected to lateral earthquake loading. Thin-Walled Struct. 158, 107145.

Berahman, F., Behnamfar, F., 2009. Probabilistic seismic demand model and fragility estimates for critical failure modes of un-anchored steel storage tanks in petroleum complexes. Probabilistic Eng. Mech. 24, 527–536.

Calayir, M., Selamet, S., Wang, Y.C., 2022. Post-earthquake fire performance of fire door sets. Fire Saf. J. 130, 103589.

Caprinozzi, S., Paolacci, F., Dolšek, M., 2020. Seismic risk assessment of liquid overtopping in a steel storage tank equipped with a single deck floating roof. J. Loss Prev. Process Ind. 67, 104269.

Casson Moreno, V., Marroni, G., Landucci, G., 2022. Probabilistic assessment aimed at the evaluation of escalating scenarios in process facilities combining safety and security barriers. Reliab. Eng. Syst. Saf. 228, 108762.

Chen, C., Reniers, G., 2020. Chemical industry in China: the current status, safety problems, and pathways for future sustainable development. Saf. Sci. 128, 104741.

Chen, C., Reniers, G., Khakzad, N., 2020. A thorough classification and discussion of approaches for modeling and managing domino effects in the process industries. Saf. Sci. 125, 104618.

Chen, G., Yang, P., Zhao, Y., Li, X., Zhao, Y., 2021. Vulnerability analysis of storage tank under the coupling effect of temperature load and blast fragment impact load. Chem. Ind. Eng. Prog. 40, 1130–1136.

Chen, G., Luo, C., Zhou, L., Rao, X., 2023. Research on three-dimensional visualization system of Natech events triggered domino accidents in oil-gas depots. J. Loss Prev. Process Ind. 81, 104953.

Cozzani, V., Reniers, G., 2013. 1 - Historical background and state of the art on domino effect assessment. In: Reniers, G., Cozzani, V. (Eds.), Domino Effects in the Process Industries. Elsevier, Amsterdam, pp. 1–10.

Cozzani, V., Salzano, E., 2004. The quantitative assessment of domino effects caused by overpressure: Part I. Probit models. J. Hazard. Mater. 107, 67–80.

Cozzani, V., Gubinelli, G., Antonioni, G., Spadoni, G., Zanelli, S., 2005. The assessment of risk caused by domino effect in quantitative area risk analysis. J. Hazard. Mater. 127, 14–30.

Cozzani, V., Gubinelli, G., Salzano, E., 2006. Escalation thresholds in the assessment of domino accidental events. J. Hazard. Mater. 129, 1–21.

Cozzani, V., Tugnoli, A., Salzano, E., 2009. The development of an inherent safety approach to the prevention of domino accidents. Accid. Anal. Prev. 41, 1216–1227.

Cozzani, V., Antonioni, G., Landucci, G., Tugnoli, A., Bonvicini, S., Spadoni, G., 2014. Quantitative assessment of domino and NaTech scenarios in complex industrial areas. J. Loss Prev. Process Ind. 28, 10–22.

D'Amico, M., Buratti, N., 2018. Observational seismic fragility curves for steel cylindrical tanks. J. Press. Vessel Technol. 141.

Ding, L., Khan, F., Ji, J., 2022. A novel vulnerability model considering synergistic effect of fire and overpressure in chemical processing facilities. Reliab. Eng. Syst. Saf. 217, 108081.
Djelosevic, M., Tepic, G., 2019. Identification of fragmentation mechanism and risk analysis due to explosion of cylindrical tank. J. Hazard. Mater. 362, 17–35.
Fabbrocino, G., Iervolino, I., Orlando, F., Salzano, E., 2005. Quantitative risk analysis of oil storage facilities in seismic areas. J. Hazard. Mater. 123, 61–69.
Fu, C., Sayed, T., 2023. Identification of adequate sample size for conflict-based crash risk evaluation: an investigation using Bayesian hierarchical extreme value theory models. Anal. Methods Accid. Res. 39, 100281.
GB50341-2014, 2014. Code for design of vertical cylindrical welded steel oil tanks. Ministry of Housing and Urban-Rural Development,, Beijing.
Ghosh, S., Ghosh, S., Chakraborty, S., 2021. Seismic fragility analysis in the probabilistic performance-based earthquake engineering framework: an overview. Int. J. Adv. Eng. Sci. Appl. Math. 13, 122–135.
Girgin, S., 2011. The natech events during the 17 August 1999 Kocaeli earthquake: aftermath and lessons learned. Nat. Hazards Earth Syst. Sci. 11, 1129–1140.
Hillier, J.K., Matthews, T., Wilby, R.L., Murphy, C., 2020. Multi-hazard dependencies can increase or decrease risk. Nat. Clim. Change 10, 595–598.
Housner, G.W., 1957. Dynamic pressures on accelerated fluid containers. Bull. Seismol. Soc. Am. 47, 15–35.
Huang, H., Chen, G., Men, J., Lai, E., 2023. Dynamic responses of steel cylindrical tanks subjected to sequential loadings of earthquake and explosion. Eng. Fail. Anal. 143, 106920.
Huang, K., Chen, G., Yang, Y., Chen, P., 2020. An innovative quantitative analysis methodology for Natech events triggered by earthquakes in chemical tank farms. Saf. Sci. 128, 104744.
Huang, M., Chen, G., Yang, P., Hu, K., Zhou, L., Men, J., Zhao, J., 2022. Multi-hazard coupling vulnerability analysis for buckling failure of vertical storage tank: Floods and hurricanes. Process Saf. Environ. Prot. 161, 528–541.
Jia, M., Chen, G., Reniers, G., 2017. An innovative framework for determining the damage probability of equipment exposed to fire. Fire Saf. J. 92, 177–187.
Jones, M.P., Weiland, K., Mitterer, C., Verdross, P., Woodward, R.T., Bismarck, A., 2023. Insights from a laboratory fire. Nat. Chem. 15, 885–889.
Khakzad, N., Amyotte, P., Cozzani, V., Reniers, G., Pasman, H., 2018. How to address model uncertainty in the escalation of domino effects? J. Loss Prev. Process Ind. 54, 49–56.
Krausmann, E., Cruz, A.M., 2013. Impact of the 11 March 2011, Great East Japan earthquake and tsunami on the chemical industry. Nat. Hazards 67, 811–828.
Krausmann, E., Renni, E., Campedel, M., Cozzani, V., 2011. Industrial accidents triggered by earthquakes, floods and lightning: lessons learned from a database analysis. Nat. Hazards 59, 285–300.
Krishnan, R., Kumar Mishra, V., Sre Adethya, V., Sivakumar, V.L., Sunagar, P., Prakash Arul Jose, J., 2023. Finite element analysis of steel frames subjected to post-earthquake fire. Mater. Today.: Proc.
Kundu, P., Majumder, S., Kar, S., Maiti, M., 2019. A method to solve linear programming problem with interval type-2 fuzzy parameters. Fuzzy Optim. Decis. Mak. 18, 103–130.
Landucci, G., Gubinelli, G., Antonioni, G., Cozzani, V., 2009. The assessment of the damage probability of storage tanks in domino events triggered by fire. Accid. Anal. Prev. 41, 1206–1215.
Li, X., 2013. Credibilistic Programming. Springer, Berlin, Heidelberg.
Li, X., Chen, G., Khan, F., Lai, E., Amyotte, P., 2022. Analysis of structural response of storage tanks subject to synergistic blast and fire loads. J. Loss Prev. Process Ind. 80, 104891.
Li, X., Chen, G., Amyotte, P., Khan, F., Alauddin, M., 2023. Vulnerability assessment of storage tanks exposed to simultaneous fire and explosion hazards. Reliab. Eng. Syst. Saf. 230, 108960.
Li, Y., Jiang, J., Zhang, Q., Yu, Y., Wang, Z., Liu, H., Shu, C.-M., 2019. Static and dynamic flame model effects on thermal buckling: Fixed-roof tanks adjacent to an ethanol pool-fire. Process Saf. Environ. Prot. 127, 23–35.
Liu, H., Jiang, J., Li, Y., Ni, L., Wang, J., 2021. Coupling effects of the explosion shock wave and heat radiation on the dynamic response of a fixed-roof tank. J. Loss Prev. Process Ind. 72, 104534.
Liu, Z.-Q., Liu, Y.-K., 2010. Type-2 fuzzy variables and their arithmetic. Soft Comput. 14, 729–747.
Lou, T., Wang, W., 2022. Mechanical properties of mild steel under combined effects of pre-damage and elevated temperatures in post-earthquake fire scenarios. J. Constr. Steel Res. 189, 107102.
Lou, T., Wang, W., Izzuddin, B.A., 2023a. A framework for performance-based assessment in post-earthquake fire: Methodology and case study. Eng. Struct. 294, 116766.
Lou, T., Wang, W., Izzuddin, B.A., 2023b. System-level analysis of a self-centring moment-resisting frame under post-earthquake fire. Eng. Struct. 289, 116294.
Mannan, S., 2012. Lees' Loss Prevention in the Process Industries, Fourth edition.,. Elsevier, Dutch.
Mannering, F.L., Bhat, C.R., 2014. Analytic methods in accident research: Methodological frontier and future directions. Anal. Methods Accid. Res. 1, 1–22.
Mayorga, S.Z., Sánchez-Silva, M., Olivar, O.J.R., Giraldo, F.M., 2019. Development of parametric fragility curves for storage tanks: A Natech approach. Reliab. Eng. Syst. Saf. 189, 1–10.
Men, J., Zhao, C., 2023. An adaptive imbalance modified online broad learning system-based fault diagnosis for imbalanced chemical process data stream. Expert Syst. Appl. 234, 121159.
Men, J., Jiang, P., Xu, H., 2019. A chance constrained programming approach for HazMat capacitated vehicle routing problem in Type-2 fuzzy environment. J. Clean. Prod. 237, 117754.
Men, J., Jiang, P., Zheng, S., Kong, Y., Zhao, Y., Sheng, G., Su, N., Zheng, S., 2020. A multi-objective emergency rescue facilities location model for catastrophic interlocking chemical accidents in chemical parks. IEEE Trans. Intell. Transp. Syst. 21, 4749–4761.
Men, J., Chen, G., Chen, P., Zhou, L., 2022a. A Gaussian type-2 fuzzy programming approach for multicrowd congestion-relieved evacuation planning. IEEE Trans. Intell. Transp. Syst. 23, 20978–20990.
Men, J., Chen, G., Yang, Y., Genserik, R., 2022b. An event-driven probabilistic methodology for modeling the spatial-temporal evolution of natural hazard-induced domino chain in chemical industrial parks. Reliab. Eng. Syst. Saf. 226, 108723.
Men, J., Chen, G., Reniers, G., Rao, X., Zeng, T., 2023a. A hybrid deep belief network-based label distribution learning system for seismic damage estimation of liquid storage tanks. Process Saf. Environ. Prot. 172, 908–922.
Men, J., Chen, G., Zeng, T., 2023b. Multi-hazard coupling effects in chemical process industry—part i: preliminaries and mechanism. IEEE Syst. J. 17, 1626–1636.
Men, J., Chen, G., Zeng, T., 2023c. Multi-hazard coupling effects in chemical process industry—part ii: research advances and future perspectives on methodologies. IEEE Syst. J. 17, 1637–1647.
Miladi, S., S. Razzaghi, M., 2019. Failure analysis of an un-anchored steel oil tank damaged during the Silakhor earthquake of 2006 in Iran. Eng. Fail. Anal. 96, 31–43.
Misuri, A., Cozzani, V., 2021. A paradigm shift in the assessment of Natech scenarios in chemical and process facilities. Process Saf. Environ. Prot. 152, 338–351.
Misuri, A., Ricci, F., Sorichetti, R., Cozzani, V., 2023. The effect of safety barrier degradation on the severity of primary natech scenarios. Reliab. Eng. Syst. Saf. 235, 109272.
Morgan J. Hurley, D.G., John, R.Hall, Kazunori, Harada, Erica, Kuligowski, Milosh, Puchovsky, José, Torero, John, M.Watts, Christopher, Wieczorek, 2016. SFPE Handbook of Fire Protection Engineering, 5th ed. Springer, New York.
Ozdemir, Z., Souli, M., Fahjan, Y.M., 2010. Application of nonlinear fluid–structure interaction methods to seismic analysis of anchored and unanchored tanks. Eng. Struct. 32, 409–423.
Qin, R., Liu, Y.-K., Liu, Z.-Q., 2011. Methods of critical value reduction for type-2 fuzzy variables and their applications. J. Comput. Appl. Math. 235, 1454–1481.
Qin, R., Zhu, J., Khakzad, N., 2020. Multi-hazard failure assessment of atmospheric storage tanks during hurricanes. J. Loss Prev. Process Ind. 68, 104325.
Ricci, F., Casson Moreno, V., Cozzani, V., 2021. A comprehensive analysis of the occurrence of Natech events in the process industry. Process Saf. Environ. Prot. 147, 703–713.
Saha, S.K., Matsagar, V., Chakraborty, S., 2016. Uncertainty quantification and seismic fragility of base-isolated liquid storage tanks using response surface models. Probabilistic Eng. Mech. 43, 20–35.
Scawthorn, C., Johnson, G.S., 2000. Preliminary report: Kocaeli (Izmit) earthquake of 17 August 1999. Eng. Struct. 22, 727–745.
Schwartz, v, 1904. Fire and Explosion Risks. Nature 71, 122–123.
Showalter, P.S., Myers, M.F., 1994. Natural disasters in the united states as release agents of oil, chemicals, or radiological materials between 1980-1989: analysis and recommendations. Risk Anal. 14, 169–182.
Spritzer, J.M., Guzey, S., 2017. Review of API 650 Annex E: Design of large steel welded aboveground storage tanks excited by seismic loads. Thin-Walled Struct. 112, 41–65.
Taghizadeh, M., Mahsuli, M., Poorzahedy, H., 2023. Probabilistic framework for evaluating the seismic resilience of transportation systems during emergency medical response. Reliab. Eng. Syst. Saf. 236, 109255.
Talebi, E., Korzen, M., Hothan, S., 2018. The performance of concrete filled steel tube columns under post-earthquake fires. J. Constr. Steel Res. 150, 115–128.
Tamascelli, N., Paltrinieri, N., Cozzani, V., 2023. Learning from major accidents: a meta-learning perspective. Saf. Sci. 158, 105984.
Theofanous, T.G., 1981. A physicochemical mechanism for the ignition of the Seveso accident. Nature 291, 640–642.
Vitorino, H., Rodrigues, H., Couto, C., 2020. Evaluation of post-earthquake fire capacity of reinforced concrete elements. Soil Dyn. Earthq. Eng. 128, 105900.
Wang, J., He, Z., Weng, W., 2020a. A review of the research into the relations between hazards in multi-hazard risk analysis. Nat. Hazards 104, 2003–2026.
Wang, M., Sun, Z., Sun, J., Cui, L., Lyu, Y., Wu, Y., 2023. Seismic fragility assessment of storage tanks considering different sources of uncertainty. Ocean Eng. 283, 114972.
Wang, Y.-H., Tang, Q., Su, M.-N., Tan, J.-K., Wang, W.-Y., Lan, Y.-S., Luo, W., Zhou, Y., 2020b. Post-earthquake fire performance of square concrete-filled steel tube columns. Thin-Walled Struct. 154, 106873.
Xu, Y., Reniers, G., Yang, M., Yuan, S., Chen, C., 2023. Uncertainties and their treatment in the quantitative risk assessment of domino effects: classification and review. Process Saf. Environ. Prot. 172, 971–985.
Yang, Y., Chen, G., Reniers, G., 2020. Vulnerability assessment of atmospheric storage tanks to floods based on logistic regression. Reliab. Eng. Syst. Saf. 196, 106721.
Zadeh, L.A., 1975. The concept of a linguistic variable and its application to approximate reasoning. Inf. Sci. 8, 199–249.
Zeng, T., Chen, G., Reniers, G., Men, J., 2022. Developing a barrier management framework for dealing with Natech domino effects and increasing chemical cluster resilience. Process Saf. Environ. Prot. 168, 778–791.
Zhou, J., Reniers, G., Cozzani, V., 2021. Improved probit models to assess equipment failure caused by domino effect accounting for dynamic and synergistic effects of multiple fires. Process Saf. Environ. Prot. 154, 306–314.
Zwillinger, D., 1992. 175 - Runge—Kutta Methods. In: Zwillinger, D. (Ed.), Handbook of Differential Equations, Second ed. Academic Press, pp. 684–690.